ICFP M2 Advanced Quantum Mechanics: Problem set #3: Bose–Hubbard model Solutions to selected questions

D.J. Papoular

November 26, 2024

1. Introduction to lattice models

1.1. Examples from numerics, physics and chemistry

1.1.1. Finite differencing: from real continuum space to a discrete lattice

We start from the hamiltonian h for a single particle in one–dimensional space:

$$h = +\frac{p^2}{2m} + v(x) = -\frac{\hbar^2}{2m}\frac{\partial^2}{\partial x^2} + v(x) \ , \tag{1}$$

where m is the mass of the particle and $v(x)$ is an external potential ensuring that the particle is trapped. The commutator $[x,p] = i\hbar$ being non–zero implies that the momentum operator p and the trapping potential operator $v(x)$ may not be simultaneously diagonalised, and the last step in Eq. (1) is written in the position basis ($|x\rangle$). In order to find the stationary states of h, we must solve the eigenvalue problem $h\,|\psi\rangle = \epsilon\,|\psi\rangle$, where the hermitian operator h acts on an infinite–dimensional Hilbert space, and the wavefunction $\psi(x)$ is defined over a continuous (i.e. uncountable) set of points, which may be an interval $[0, L]$ of real values for a system of finite size L, or all real numbers in the case of a scattering problem. For some specific (and rare) cases of $v(x)$, the Schrödinger Eq. (1) may be solved explicitly. In most cases, no explicit solution is available, and we must turn to numerical approaches.

In this section, we consider one popular and elementary numerical approach called the *finite–diference method*. Our goal is to show that this method amounts to replacing the continuum–space problem described by the Hamiltonian h by a lattice model.

In the finite–difference method, we relinquish the description of $\psi(x)$ over an uncountable set of values of x. Instead, we sample the wavefunction $\psi(x_n)$ over a finite set of positions $(x_n)_{1\leq n\leq N}$. Let us assume that the x_n are regularly spaced: $x_n = na$. Then, if a is small enough, an approximation for $\psi''(x_n)$ may be obtained through:

$$\psi''(x_n) \approx \frac{1}{a^2}\left(\psi(x_{n+1}) - 2\psi(x_n) + \psi(x_{n-1})\right) \ . \tag{2}$$

Hence, we may approximate the exact eigenvalue equation $h\,|\psi\rangle = \epsilon\,|\psi\rangle$ by the following one:

$$\epsilon\,\psi_n = -\frac{\hbar^2}{2ma^2}\left(\psi_{n+1} - 2\psi_n + \psi_{n-1}\right) + v_n\psi_n \ . \tag{3}$$

Equation (3) does not fully specify the finite–differencing problem: it must be assorted with a boundary condition which guarantees the hermiticity of the approximate hamiltonian operator.

Strict boundary conditions, $\psi_0 = \psi_{N+1} = 0$, are applicable if the system is trapped in between two impenetrable walls at $x = 0$ and $x = (N+1)a$. Periodic boundary conditions, $\psi_0 = \psi_{N+1}$ with no specific value being imposed, are often the most convenient choice if it makes sense to interpret the potential $v(x)$ as a periodic function with period Na ($v(0) = v(Na)$), which is the case e.g. if the particle is constrained to move on a ring of perimeter Na. We focus on the case of periodic boundary conditions. Then, the finite–difference equation amounts to approximating h by the $N \times N$ matrix h_{FD} expressed in the discrete position basis $(|x_n\rangle)$:

$$h_{\mathrm{FD}} = +\frac{\hbar^2}{ma^2}\mathbb{1} \quad -\frac{\hbar^2}{2ma^2}\begin{bmatrix} 0 & 1 & 0 & 0 & 1 \\ 1 & \ddots & 1 & 0 & 0 \\ 0 & \ddots & \ddots & \ddots & 0 \\ 0 & 0 & 1 & \ddots & 1 \\ 1 & 0 & 0 & 1 & 0 \end{bmatrix} + \begin{bmatrix} v_1 & 0 & 0 & 0 & 0 \\ 0 & \ddots & 0 & 0 & 0 \\ 0 & 0 & \ddots & 0 & 0 \\ 0 & 0 & 0 & \ddots & 0 \\ 0 & 0 & 0 & 0 & v_N \end{bmatrix} . \tag{4}$$

The matrix h_{FD} encompasses both Eq. (3) and the periodic boundary condition $\psi_0 = \psi_N$, the latter being encoded by the two ones appearing in red at the top right and bottom left corners of the matrix proportional to $-\hbar^2/(2ma^2)$ on the right–hand side (for strict boundary conditions $\psi_0 = \psi_N = 0$, both of these matrix elements would be 0.). It is hermitian and, hence, may be diagonalised through all the usual methods (for example, on the computer, using a package for numerical linear algebra such as LAPACK or its variants).

The matrix form of Eq. (4) is the one which should be coded when performing numerical simulations on a computer. We shall now recast it in a form which allows for an interpretation in terms of a lattice model. First, the term $\hbar^2/(ma^2)\mathbb{1}$ is a constant energy shift which has no consequence, and we drop it from now on. Next, we introduce the kets $|n\rangle = |x_n\rangle$, so that the set $(|n\rangle)_{1\leq n\leq N}$ is a basis of the N–dimensional Hilbert space on which h_{FD} acts. We enforce the periodic boundary conditions by setting $|0\rangle = |N\rangle$ and $|N+1\rangle = |1\rangle$. Equation (4) may now be written in braket notation:

$$h_{\mathrm{FD}} = -J\sum_{n=1}^{N}\left(|n+1\rangle\langle n| + |n-1\rangle\langle n|\right) \quad + \sum_{n=1}^{N} v_n |n\rangle\langle n| \ , \tag{5}$$

where the positive number $J = +\hbar^2/(2ma^2)$ is called the hopping amplitude. Equation (5) exhibits two typical features of a lattice model. First, it is defined in terms of a finite set of position kets $|n\rangle$ which represent the *discrete* lattice sites. Second, it includes a *hopping term* which describes how the particle may move from the site $|n\rangle$ to one of its nearest–neighbouring sites $|n+1\rangle$ or $|n-1\rangle$. The hopping amplitude $t > 0$ appears with a minus sign in h_{FD}, meaning that, in the absence of any trapping potential, it is energetically favourable for the particle to be delocalised over many sites. The second sum on the right–hand side of Eq. (5) represents the trapping potential, which is diagonal in terms of the sites $|n\rangle$, just like the trapping potential $v(x)$ is diagonal in the position basis $|x\rangle$ in continuum space. The Hamiltonian h_{FD} is expressed in first quantisation, so that it is not straightforward to include a two–body interaction term: this will be done below in terms of creation and annihilation operators.

In the absence of a trapping potential, $v_1 = \ldots = v_N = 0$. Then, h_{FD} is a circulant matrix whose eigenvalues are the energies $\epsilon_p^{\mathrm{FD}} = -2J\cos(k_p a)$ with $k_p a = 2\pi\, p/N$ (see Sec. 2.1 for another derivation of this result in terms of Bloch's theorem).

1.1.2. Benzene molecule

1.2. Bloch's theorem

We consider the (single–particle) Hamiltonian $h = \boldsymbol{p}^2/(2m) + v(\boldsymbol{r})$, where the potential $v(\boldsymbol{r})$ is spatially periodic. Its spatial periodicity is encided by the direct lattice vectors $(\boldsymbol{a}_i)_{1\leq i\leq 3}$: for all positions $\boldsymbol{r}$ and all three direct lattice vectors $\boldsymbol{a}_i$, $v(\boldsymbol{r}+\boldsymbol{a}_i) = v(\boldsymbol{r})$. Then, a basis of eigenstates

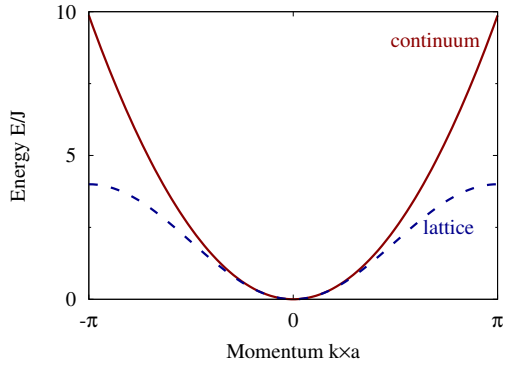

Figure 1 Dispersion relations $\epsilon_k = \hbar^2 k^2/2m$ in free space (solid red) and $\epsilon_p^{\mathrm{FD}} = 2J(1-\cos(ka))$ (dashed blue) for the lattice model obtained by finite differences (Eq. (5)). Momenta are in units of the inverse lattice spacing $1/a$ and energies in units of the hopping amplitude J. The two dispersion relations coincide for small $|ka| \ll 1$, i.e. the discretised model captures phenomena whose wavelengths are greater than a. They differ for larger momenta $|ka| \lesssim \pi$, i.e. the discretised model does not resolve higher–energy phenomena whose wavelengths are $\lesssim a$.

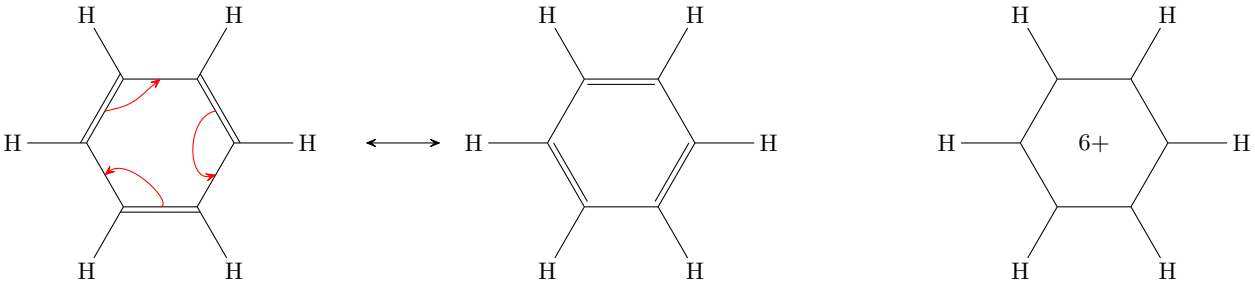

Figure 2 Left: the two configurations for benzene taking part in the resonance describing the three delocalised double bonds. Right: a fictitious 'benzene ion', charged 6+, where all six electrons responsible for the double bonds have been removed. A quantum mechanical model for the molecule may be obtained by viewing the six carbon atoms on the ring as a six–site Fermi–Hubbard model where each site may accommodate up to two electrons with opposite spins.

of H may be found such that each eigenstate $|\psi\rangle$ is the product of a plane wave $\exp(i\boldsymbol{q}\cdot\boldsymbol{r})$ *with a function $u(\boldsymbol{r})$ which has the same spatial period as the lattice potential v*:

$$\psi(\boldsymbol{r}) = e^{i\boldsymbol{q}\cdot\boldsymbol{r}}\, u(\boldsymbol{r}), \quad \text{with} \quad u(\boldsymbol{r}+\boldsymbol{a}_i) = u(\boldsymbol{r}) \quad \text{for all positions } \boldsymbol{r} \text{ and all three vectors } \boldsymbol{a}_i. \tag{6}$$

The Bloch wavefunctions of Eq. (6) are eigenstates of h, i.e. they correspond to a well–defined energy ϵ such that $h\,|\psi\rangle = \epsilon\,|\psi\rangle$. They correspond to the plane–wave eigenstates $e^{iqx}/\sqrt{V}$ of a single particle in free space (which they reduce to if the potential v is adiabatically turned off). Hence, *they extend over the whole lattice*, just like the plane waves extend over the whole volume. In free space, we may also define the position states $|\boldsymbol{r}\rangle$, which are localised at the point $\boldsymbol{r}$ but *are not stationary states* of the free particle Hamiltonian $\boldsymbol{p}^2/(2m)$. Similarly, in the presence of the periodic potential, we may define wavefunctions which are localised in a given lattice site $|\boldsymbol{j}\rangle$, which are labelled by the integer multiplet $\boldsymbol{j} = (j_1, j_2, j_3)$. These localised states are called *Wannier functions*[1]. They are linear combinations of Bloch functions corresponding to different energies within a given band b, hence, they *are not stationary states* of the Hamiltonian h.

We first prove the theorem in 1D, where there is no need to discuss the reciprocal lattice, which makes the proof particularly transparent. Then, we turn to the 3D case. We first define the reciprocal lattice and explain its meaning in terms of duality. Finally, we prove Bloch's theorem in 3D, following the lines of the 1D proof and emphasizing the role of the reciprocal lattice.

[1] Wannier functions should be manipulated with great care. For primitive lattices, i.e. lattices whose unit cell contains exactly one minimum, the Bravais functions $w_{0\boldsymbol{j}}$ corresponding to the lowest band ($b = 0$) and to the site $\boldsymbol{j}$ centred at the position $\boldsymbol{r}_{\boldsymbol{j}}$, may be chosen to be real and to satisfy $w_{0\boldsymbol{j}}(\boldsymbol{r}) = w_0(\boldsymbol{r} - \boldsymbol{r}_{\boldsymbol{j}})$. Even in this simple case, difficulties arise from the non–trivial decay of $w_0(\boldsymbol{r})$ outside the lattice site [1, §II.B]. If the unit cell contains multiple minima (e.g. in the case of a lattice of double wells), the construction of Wannier functions is challenging and crucially hinges on the choice of the phases in the linear combination of Bloch wavefunctions.

1.2.1. Proof of Bloch's theorem in 1D.

We introduce the translation operator $T_a = \exp(-iap/\hbar)$ corresponding to the spatial period a. Its action on the position basis vectors $|x\rangle$ reads $T_a |x\rangle = |x + a\rangle$. The assumption that v be periodic with period a means that the Hamiltonian $[h, T_a] = 0$. Therefore, there is a basis of states $|\psi\rangle$ which are eigenvectors of h and T_a simultaneously:

$$h |\psi\rangle = \epsilon |\psi\rangle \quad \text{and} \quad T_a |\psi\rangle = \tau |\psi\rangle \ . \tag{7}$$

The operator T_a is unitary, therefore all its eigenvalues τ are complex numbers of modulus 1. Hence, we may always write $\tau = e^{-iaq}$, where q is a real number. We project the eigenvalue equation for T_a (i.e. the second relation in Eq. (7)) onto the basis x:

$$\langle x|T_a|\psi\rangle = e^{-iqa} \langle x|\psi\rangle \ . \tag{8}$$

The operator T_a is unitary, so that $T_a^\dagger = T_a^{-1} = T_{-a}$. Therefore,

$$\langle x| T_a = \left(T_a^\dagger |x\rangle\right)^\dagger \quad = (T_{-a} |x\rangle)^\dagger \quad = (|x - a\rangle)^\dagger \quad = \langle x - a| \ . \tag{9}$$

Hence, the eigenvalue Eq. (8) reduces to:

$$\psi(x - a) = e^{-iqa} \psi(x) \ . \tag{10}$$

We now call $\psi(x) = \psi_q(x)$, and introduce the function $u_q(x) = \psi_q(x)e^{-iqx}$. Replacing $\psi_q(x)$ in terms of $u_q(x)$ in Eq. (10), we conclude that $u_q(x - a) = u_q(x)$, which proves the theorem in 1D.

The wavevector q appearing in Eq. (8) is defined up to any integer multiple of $2\pi/a$. In other words, the functions ψ_q and $\psi_{q+2\pi/a}$ must represent the same quantum state. Hence, ψ_q and $\psi_{q+2\pi/a}$ must be equal up to an irrelevant constant phase, and the corresponding energies $\epsilon_q = \epsilon_{q+2\pi/a}$ should be equal. *We choose the following convention:*

$$\psi_{q+2\pi/a} = \psi_q \ , \qquad \text{which is equivalent to:} \qquad u_{q+2\pi/a}(x) = \exp(-i2\pi x/a)\, u_q(x) \ . \tag{11}$$

Thus, the independent functions ψ_q (or u_q) are those for which $q \in]-\pi/a, \pi/a]$ (first Brillouin zone), and the dispersion relation ϵ_q is a periodic function of q with the period $2\pi/a$.

1.2.2. Crystal lattices in 3D: reciprocal lattice and duality

In the usual 3D Euclidean space of elementary geometry, no physical units are invoked, and we may introduce an orthonormal basis $(\boldsymbol{e}_i)_{1\leq i\leq 3}$ by the requirement that $\boldsymbol{e}_i \cdot \boldsymbol{e}_j = \delta_{ij}$. Orthonormal bases are particularly convenient because they make it straightforward to extract the component of any vector $\boldsymbol{v} = \sum_i v_i \boldsymbol{e}_i$ along the basis vector $\boldsymbol{e}_{i_0}$, which may be expressed as a scalar product:

$$v_{i_0} = \boldsymbol{e}_{i_0} \cdot \boldsymbol{v}, \quad \text{or equivalently:} \quad \boldsymbol{v} = \sum_{i=1}^{3} \boldsymbol{e}_i \, (\boldsymbol{e}_i \cdot \boldsymbol{v}), \quad \text{that is,} \qquad |\boldsymbol{v}\rangle = \left(\sum_{i=1}^{3} |\boldsymbol{e}_i\rangle \langle \boldsymbol{e}_i| \right) |\boldsymbol{v}\rangle \ . \tag{12}$$

In the third version of Eq. (12), we have introduced the bra–ket notation so as to highlight that this property is actually the closure relation familiar from quantum mechanics.

In the context of periodic crystalline lattices, the straightforward Eq. (12) is not applicable, for two reasons. Both are linked to the fact that we wish our system of basis vectors, now called $(\boldsymbol{a}_i)_{1\leq i\leq 3}$, to encode the spatial periodicity of the lattice. First, the vectors $\boldsymbol{a}_i$ encode the spatial extent of the unit cell. Hence, their moduli carry the unit of length. Thus, the scalar product $\boldsymbol{a}_i \cdot \boldsymbol{a}_i$ has the dimension of a length squared, whereas δ_{ij} is dimensionless, so that the vectors $\boldsymbol{a}_i$ may not be chosen to be normalised. Second, the basis vectors $(\boldsymbol{a}_i)$ need not be orthogonal: they are for a cubic unit cell, but in the general case they are not. In particular, they are not orthogonal in the ubiquitous hexagonal close–packing lattice geometry.

The extraction of the components (x_i) of an arbitrary position vector $\boldsymbol{r} = \sum_{i=1}^{3} x_i \boldsymbol{a}_i$ in the basis $\boldsymbol{a}_i$ requires the calculation of the inverse of the Gram matrix G:

$$\begin{pmatrix} x_1 \\ x_2 \\ x_3 \end{pmatrix} = G^{-1} \begin{pmatrix} \boldsymbol{a}_1 \cdot \boldsymbol{x} \\ \boldsymbol{a}_2 \cdot \boldsymbol{x} \\ \boldsymbol{a}_3 \cdot \boldsymbol{x} \end{pmatrix} \quad \text{where the } 3 \times 3 \text{ Gram matrix is} \quad (G_{ij}) = (\boldsymbol{a}_i \cdot \boldsymbol{a}_j) \ . \tag{13}$$

The 3×3 matrices G and G^{-1} characterise the geometry of the unit cell. They may be calculated once and for all as soon as the lattice structure is given. This is not a taxing step.

We now provide a geometrical interpretation for the matrix G^{-1}, which allows us to write Eq. (13) in a form almost as simple as Eq. (12). We introduce the three vectors $(\boldsymbol{b}_i)_{1 \leq i \leq 3}$ whose components in the basis $(\boldsymbol{a}_k)$ correspond to the lines of the inverse Gram matrix $G = (G_{ik}^{-1})$:

$$\boldsymbol{b}_i = 2\pi \sum_{k=1}^{3} G_{ik}^{-1} \, \boldsymbol{a}_k \ . \tag{14}$$

This is equivalent to defining the basis $(\boldsymbol{b}_i)_{1 \leq i \leq 3}$ as the dual basis of $(\boldsymbol{a}_i)_{1 \leq i \leq 3}$. Indeed:

$$\boldsymbol{b}_i \cdot \boldsymbol{a}_j \quad = 2\pi \sum_{k=1}^{3} G_{ik}^{-1} \, \boldsymbol{a}_k \cdot \boldsymbol{a}_j \quad = 2\pi \sum_{k=1}^{3} G_{ik}^{-1} G_{kj} \quad = 2\pi \, \delta_{ij} \ , \tag{15}$$

where the second–to–last step follows from the definition of the Gram matrix elements $G_{kj} = \boldsymbol{a}_k \cdot \boldsymbol{a}_j$, and the last step is the statement $G^{-1}G = \mathbb{1}$. The presence of the extra factor 2π will be justified shortly. In terms of the vectors $(\boldsymbol{b}_i)$, Eq. (13) reads:

$$x_{i_0} = \frac{\boldsymbol{b}_{i_0} \cdot \boldsymbol{r}}{2\pi}, \quad \text{or equivalently:} \quad \boldsymbol{r} = \sum_{i=1}^{3} \boldsymbol{a}_i \frac{\boldsymbol{b}_i \cdot \boldsymbol{r}}{2\pi}, \quad \text{that is,} \quad |\boldsymbol{r}\rangle = \left(\frac{\sum_{i=1}^{3} |\boldsymbol{a}_i\rangle \langle \boldsymbol{b}_i|}{2\pi} \right) |\boldsymbol{r}\rangle \ . \tag{16}$$

The third version of Eq. (16) is very similar to the standard closure relation of Eq. (12). The only difference is that it now involves the sum $\sum_i |\boldsymbol{a}_i\rangle \langle \boldsymbol{b}_i|$, where the kets contain the *direct–lattice vectors* $\boldsymbol{a}_i$ whereas the bras contain the *reciprocal lattice vectors* $\boldsymbol{b}_i$.

This geometrical interpretation has a physical meaning. First, the moduli $|\boldsymbol{a}_i|$ all have the dimension of a length, whereas the moduli $|\boldsymbol{b}_i|$ all have the dimension of an inverse length, i.e. of a wavevector. Hence, though the bases $(\boldsymbol{a}_i)_{1 \leq i \leq 3}$ and $(\boldsymbol{b}_i)_{1 \leq i \leq 3}$ both span three–dimensional vector spaces, these spaces do not coincide. Equation (14) shows that the basis $(\boldsymbol{b}_i)_{1 \leq i \leq 3}$ actually spans the vector space which is *dual* to position space, hence the name 'reciprocal lattice vectors' given to the vectors $(\boldsymbol{b}_i)$. Second, let us focus on the positions $\boldsymbol{r} = \sum_i x_i \boldsymbol{a}_i$ and wavevectors $\boldsymbol{k} = \sum_i k_i \boldsymbol{b}_i$ whose components (x_i) or (k_i) are integers. In both cases, we obtain a lattice, i.e. a discrete set of points endowed with the symmetries of the crystal. The positions with integer components each correspond to an atom, and they are all equivalent from the point of view of the symmetry of the crystal lattice (i.e. they all transform one into the other). The momenta with integer coefficients also play a key role: they are those which enter in the Fourier series of a function of position $u(\boldsymbol{r})$ with the periodicity of the crystal lattice. Indeed, let us Fourier–expand $u(\boldsymbol{r})$:

$$u(\boldsymbol{r}) = \sum_{\boldsymbol{k}} c_{\boldsymbol{k}} e^{i\boldsymbol{k} \cdot \boldsymbol{r}} \ . \tag{17}$$

The periodicity of u imposes $u(\boldsymbol{r} + \boldsymbol{a}_j) = u(\boldsymbol{r})$ for all three vectors $(\boldsymbol{a}_j)_{1 \leq j \leq 3}$, so that all wavevectors $\boldsymbol{k}$ appearing in the sum of Eq. (17) must satisfy $\exp(i\boldsymbol{k} \cdot \boldsymbol{a}_j)$ for $1 \leq j \leq 3$, so that $\boldsymbol{k} \cdot \boldsymbol{a}_j = 2\pi n_j$, with n_j being an integer. We write $\boldsymbol{k} = \sum_i k_i \boldsymbol{b}_j$. Then, using the duality Eq. (15), we find $\boldsymbol{k} \cdot \boldsymbol{a}_j = 2\pi k_j$, so that $k_j = n_j$ is an integer. This is why the definition of Eqs. (14) and (15) for the dual basis $(\boldsymbol{b}_j)$ includes an additional factor 2π with respect to the usual mathematical definition.

Hence, the *real–space basis* $(\boldsymbol{a}_i)$ is the natural one for position vectors $\boldsymbol{r}$, whereas the *reciprocal–space basis* $(\boldsymbol{b}_i)$ is the natural one for wavevectors $\boldsymbol{k}$. In particular, in the expansions $\boldsymbol{r} = \sum_i x_i \boldsymbol{a}_i$ and $\boldsymbol{k} = \sum_i k_i \boldsymbol{b}_i$, the components x_i and k_i are all dimensionless.

Similar duality properties appear in many other theories. They are usually represented in terms of the covariant and contravariant components of tensors, of which kets and bras are one example. Two other famous examples are the covariant and contravariant components of four–vectors in special relativity, and of spinors representing the wavefunctions of particles with arbitrary spin.

1.2.3. Proof of Bloch's theorem in 3D.

In this section, we extend the proof of Sec. 1.2.1 to the 3D case. We now need three translation operators $T_{\boldsymbol{a}_j} = \exp(-i\boldsymbol{a}_j \cdot \boldsymbol{p}/\hbar)$, corresponding to the three direct–lattice basis vectors $(\boldsymbol{a}_j)_{1\leq j\leq 3}$. These three operators commute with one another, $[T_{\boldsymbol{a}_i}, T_{\boldsymbol{a}_j}] = 0$, because the three momentum operators do so, $[p_i, p_j] = 0$. Furthermore, the assumption of three–dimensional periodicity means that the commutator $[h, T_{\boldsymbol{a}_i}] = 0$ for each of the three $T_{\boldsymbol{a}_i}$. To sum up, all four operators h and $(T_{\boldsymbol{a}_j})_{1\leq j\leq 3}$ commute with one another. Hence, there exists a basis of eigenstates where all four of them are simultaneously diagonal:

$$h\,|\psi\rangle = \epsilon\,|\psi\rangle \quad \text{and, for } 1 \leq j \leq 3, \quad T_{\boldsymbol{a}_j}\,|\psi\rangle = \tau_j\,|\psi\rangle \ . \tag{18}$$

The three operators $T_{\boldsymbol{a}_j}$ are unitary, so that all three eigenvalues τ_j are complex numbers of modulus 1. Thus, we write $\tau_j = \exp(-i2\pi\, q_j)$, where the q_j's are three real numbers. We introduce the following wavevector $\boldsymbol{q}$, defined in terms of the q_j's in the reciprocal lattice basis $(\boldsymbol{b}_j)_{1\leq j\leq 3}$:

$$\boldsymbol{q} = \sum_{j=1}^{3} q_j\,\boldsymbol{b}_j \ . \tag{19}$$

Thanks to the duality Eq. (15), this wavevector satisfies:

$$\boldsymbol{q}\cdot\boldsymbol{a}_i = \sum_{j=1}^{3} q_j\,\boldsymbol{b}_j\cdot\boldsymbol{a}_i = 2\pi\, q_i \ , \tag{20}$$

so that the three eigenvalue equations for the translation operators now read:

$$T_{\boldsymbol{a}_j}\,|\psi\rangle = e^{-i\boldsymbol{q}\cdot\boldsymbol{a}_j}\,|\psi\rangle \quad \text{for } 1 \leq j \leq 3. \ . \tag{21}$$

The end of the proof is very similar to the 1D case of Sec. 1.2.1. We project Eq. (21) onto the position basis $|\boldsymbol{r}\rangle$ to find:

$$\psi(\boldsymbol{r} - \boldsymbol{a}_j) = e^{-i\boldsymbol{q}\cdot\boldsymbol{a}_j}\,\psi(\boldsymbol{r}) \ . \tag{22}$$

We define the function $u(\boldsymbol{r}) = \exp(-i\boldsymbol{q}\cdot\boldsymbol{r})\psi(\boldsymbol{r})$. Expressing Eq. (22) in terms of u, we find $u(\boldsymbol{r} - \boldsymbol{a}_j) = u(\boldsymbol{r})$ for all three lattice vectors $\boldsymbol{a}_j$, which concludes the proof of the theorem in 3D.

Similarly to the 1D case, the wavevector $\boldsymbol{q}$ labelling the Bloch wave $\psi_{\boldsymbol{q}}$ is defined up to a reciprocal lattice vector $\boldsymbol{k}$, meaning that the Bloch waves $\psi_{\boldsymbol{q}}$ and $\psi_{\boldsymbol{q}+\boldsymbol{k}}$ represent the same quantum state. Hence, $\psi_{\boldsymbol{q}}$ and $\psi_{\boldsymbol{q}+\boldsymbol{k}}$ should be equal up to a constant phase, and the corresponding energies $\epsilon_{\boldsymbol{q}} = \epsilon_{\boldsymbol{q}+\boldsymbol{k}}$ must be equal. *We choose the following convention:*

$$\psi_{\boldsymbol{q}+\boldsymbol{k}} = \psi_{\boldsymbol{q}} \ , \qquad \text{which is equivalent to:} \qquad u_{\boldsymbol{q}+\boldsymbol{k}}(\boldsymbol{r}) = \exp(-i\boldsymbol{k}\cdot\boldsymbol{r})\,u_{\boldsymbol{q}(\boldsymbol{r})} \ . \tag{23}$$

Thus, the independent Bloch wavefunctions $\psi_{\boldsymbol{q}}$ are those for which $\boldsymbol{q}$ lies in the first Brillouin zone (or any other set of wavevectors compatible with the periodicity of the reciprocal lattice), and the dispersion relation $\epsilon_{\boldsymbol{q}}$ is a periodic function of the wavevector $\boldsymbol{q}$ whose period in momentum–space coincides with that of the reciprocal lattice.

1.3. Band structure

We now briefly describe the impact of the spatial periodicity of the single–particle Hamiltonian h on the single–particle energy spectrum. We focus on the case of a separable potential, $v(\boldsymbol{r}) = v_x(x) + v_y(y) + v_z(z)$. This assumption is not necessary, but it simplifies the analysis, because the

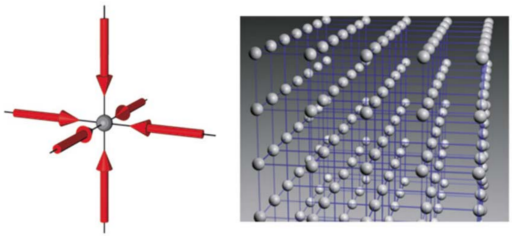

Figure 3 Generation of a 3D square optical lattice. Along each of the three spatial directions x, y, z, two propagating laser beams (or one retroreflected beam) interfere to create a standing wave. The atoms are confined near the nodes of the standing wave for blue–detuned laser beams ($\omega_L > \omega_A$) and near the antinodes for red–detuned laser beams ($\omega_L > \omega_A$). Reproduced from Ref. [1].

single–particle eigenstates of h, $\psi(\boldsymbol{r})$, may be sought in the form of products of 1D wavefunctions, $\psi(\boldsymbol{r}) = \psi_x(x)\psi_y(y)\psi_z(z)$, each of which is an eigenstate of the 1D Hamiltonians

$$h_x = \frac{p_x^2}{2m} + v_x(x) \ , \quad h_y = \frac{p_y^2}{2m} + v_y(y) \ , \quad h_z = \frac{p_z^2}{2m} + v_z(x) \ . \tag{24}$$

Such a factorisation is available for e.g. the standard 3D cubic lattice generated thanks to three retro–reflected laser beams with equal wavelengths λ (see Fig. 3), in which case:

$$v(\boldsymbol{r}) = v_{0x}\sin^2(q_R x) + v_{0y}\sin^2(q_R y) + v_{0z}\sin^2(q_R z) \ , \tag{25}$$

In Eq. (25), the recoil momentum $\hbar q_R$, defined by $q_R = 2\pi/\lambda$, defines the lattice parameter a, i.e. the spatial period along all three directions x, y, z, through $a = \pi/q_R = \lambda/2$. The factorisation is *not applicable* for more complicated cases such as the 2D hexagonal (also called 'triangular') lattice or the honeycomb lattice.

Hence, we specialise our analysis to the potential of Eq. (25), and exploit separability to reduce the problem to the following 1D single–particle Hamiltonian:

$$h_x = \frac{p_x^2}{2m} + v_0\sin^2(q_R x) \ . \tag{26}$$

We now describe a method, presented e.g. in Ref. [2, Sec. 3.1], allowing for the numerical calculation of the eigenfunctions and eigenvalues of h_x. Thanks to Bloch's theorem (see Sec. 1.2), we seek the eigenstates of h_x as Bloch waves ψ_{qb}, with $\hbar q$ being the quasi–momentum and b the band index:

$$\psi_{qb}(x) = e^{iqx}u_{qb}(x) \ , \qquad \text{where} \qquad u_{qb}(x+a) = u_{qb}(x) \ . \tag{27}$$

The function u_{qb} is periodic, hence, it may be expanded into a Fourier series. Its spatial period is $a = \pi/q_R$, so that the relevant plane waves are those with periods a/j, with j being an integer:

$$u_{qb}(x) = \sum_{j\in\mathbb{Z}} c_j \exp\left[i\,j\frac{2\pi}{a}\,x\right] \ , \qquad \text{so that} \qquad \psi_{qb}(x) = \sum_{j\in\mathbb{Z}} c_j \exp\left[i\left(q + j\frac{2\pi}{a}\right)x\right] \ . \tag{28}$$

The coefficients c_j must now be chosen such that $|\psi_{qb}\rangle$ is an eigenstate of h_x. Let ϵ be the corresponding eigenvalue, so that the Schrödinger equation reads:

$$\epsilon\,\psi_{qb}(x) = -\frac{\hbar^2}{2m}\psi''_{qb}(x) + v_0\sin^2(kx)\psi_{qb}(x) \ . \tag{29}$$

Injecting Eq. (28) into Eq. (29), we obtain an equation on the coefficients c_j:

$$\frac{\epsilon}{\epsilon_R}\,c_j \ = \ \left[\left(2j + \frac{q}{q_R}\right)^2 + \frac{v_0}{2\epsilon_R}\right]c_j \ - \ \frac{v_0}{4\epsilon_R}(c_{j-1} + c_{j+1}) \ , \tag{30}$$

where the recoil energy $\epsilon_R = \hbar^2 q_R^2/(2m)$. Hence, the periodic character of the Bloch function $u_{qb}(x)$ has allowed us to replace the differential eigenvalue problem of Eq. (29) by the *matrix eigenvalue problem* of Eq. (30), which involves the discrete set of coefficients (c_j). For a given value

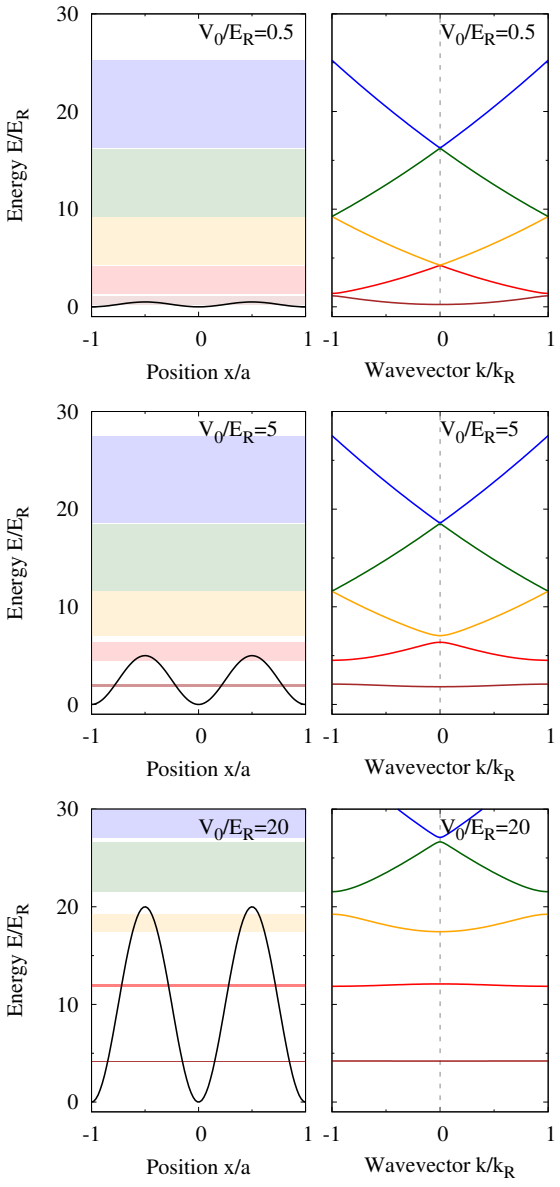

Figure 4 Band structure for the lattice potential $V(x) = V_0 \sin^2(\pi x/a)$, whose spatial period is a. Lengths are expressed in units of a, wavevectors in units of the recoil wavevector $q_R = \pi/a$, and energies in units of the recoil energy $E_R = \hbar^2 q_R^2/(2m)$. The two top graphs show the band structure for the small lattice amplitude $V_0/E_R = 0.5$, where the effect of the potential is a perturbative opening of small gaps at the edges of the Brillouin zone, i.e. near $q = \pm q_R$ (free particle limit). The two bottom graphs show the band structure for the large lattice amplitude $V_0/E_R = 20$, where the first two bands, corresponding to energies $\ll E_R$, are nearly flat because of the negligible tunnelling between the lattice sites (atomic limit). The two graphs on the middle line show the band structure for V_0/E_R, away from these two limits. In all cases, the left panel shows the periodic potential in terms of the real–space coordinate x (black) and the spread in energies for the first five bands (coloured shaded areas), whereas the right panel shows the dependence of the energies in each band on the wavevector q.

of q, the 'matrix' $(\mathfrak{h}_{ij}) = (\mathfrak{h}_{ij}(q))$ involved in Eq. (30) is infinite in both directions $i, j \to \pm\infty$. Its coefficients satisfy:

$$\mathfrak{h}_{jj} = \left(2j + \frac{q}{q_R}\right)^2 + \frac{v_0}{2\epsilon_R} \ , \qquad \mathfrak{h}_{j-1,j} = \mathfrak{h}_{j+1,j} = -\frac{v_0}{4\epsilon_R} \ , \qquad \mathfrak{h}_{ij} = 0 \text{ for } |i-j| \geq 2. \tag{31}$$

Hence, $(\mathfrak{h}_{ij})$ is real, symmetric, and tridiagonal. Its first few eigenvectors and eigenvalues may be found by truncating it to a finite–sized matrix, i.e. by replacing $(\mathfrak{h}_{ij})$ with $(\tilde{\mathfrak{h}}_{ij})$ such that $\tilde{\mathfrak{h}}_{ij} = \mathfrak{h}_{ij}$ for $-p \leq i, j \leq p$ and $\tilde{\mathfrak{h}}_{ij} = 0$ otherwise. Then, $(\tilde{\mathfrak{h}}_{ij})$ is a $(2p+1) \times (2p+1)$ matrix which may be diagonalised using the usual methods, yielding $(2p+1)$ real eigenvalues and eigenvectors. The low–energy eigenelements of $(\tilde{\mathfrak{h}}_{ij})$ are good approximations to those of $(\mathfrak{h}_{ij})$. A given eigenvector of $(\tilde{\mathfrak{h}}_{ij})$ is an acceptable approximation if its components c_j decrease sufficiently rapidly for $|j| < p$. By contrast, if c_p or c_{-p} are not found to be very small, then this eigenvector (and all those with higher energies) should be discarded and recalculated using a larger value for the cutoff p.

This method allows for the calculation of the first few eigenvalues $(\epsilon_b(q))$ of $(\mathfrak{h}_{ij}(q))$, sorted by increasing energies $\epsilon_1(q) < \epsilon_1(q) < \dots$. The set of energies $\epsilon_1(q)$ for all values of q make up the first band (shown in dark red in Fig. 4 for various values of the lattice depth V_0/E_R); the set of $\epsilon_2(q)$ make up the second band (red), ... and the set of $\epsilon_b(q)$ make up the band of index b.

The listing 1 shows the short Python script, implementing this algorithm, which was used to produce Fig. 4; the listing 2 allows for a straighforward visualisation of the results using Matplotlib.

1.3.1. Interpretation of the band structure in two limiting cases

The band structure obtained with the periodic 1D potential of Eq. (26) is shown on Fig. 4 for various values of the lattice height v_0. These dispersion relations may be understood through simple arguments in two different limits: *(i)* the shallow lattice limit and *(ii)* the atomic limit.

Shallow lattice limit. This case corresponds to a lattice depth $v_0 \ll \epsilon_R$ which is small compared to the recoil energy ϵ_R. It is illustrated by the two panels on the top line of Fig. 4. Deep in this limit, the periodic potential no longer plays any role, and the dispersion relation $\epsilon(q) = \hbar^2 q^2/(2m)$ is the usual single parabola characteristic of a single particle in free space (Fig. 5, left panel). It is defined for all wavevectors q and exhibits a single branch. One may also understand this dispersion relation in a different way which is compatible with the presence of a weak periodic potential. In this second picture, the various relevant parts of the parabola are folded into the first Brillouin zone $-q_R < q \leq q_R$ (Fig. 5, right panel). Then, the dispersion relation is defined only for wavevectors belonging to the first Brillouin zone, but it exhibits multiple branches, each of which corresponds to a band. For nonvanishing lattice amplitudes $v_0 > 0$, a small energy gap opens up at the edges of each band (where the color code changes on Fig. 5).

"Atomic limit". We consider a band which is such that the energies of all of its states are small compared to v_0 (for instance, the band represented in brown on the bottom line of Fig. 4). Then, the tunnelling between the different sites of the lattice are negligible, as illustrated on Fig. 6. Hence, all sites are nearly uncoupled, a situation which has historically been termed 'atomic limit' by condensed–matter physicists (though each well may contain more than one atom!). Then, the translational symmetry of the problem ensures that all sites support a state with nearly the same energy, giving rise to N_L nearly–degenerate states (represented in red on Fig. 6). The very weak tunnel coupling turns these degenerate states into a narrow band with a very small spread in energies, i.e. a nearly flat band. Accordingly, the lowest–energy (brown) band is nearly invisible on the bottom left panel of Fig. 4.

In this limit, the Bloch wavefunctions $|\psi_{0k}\rangle$ belonging to the deep band $b = 0$ may be expressed exactly in terms of the wavefunctions of the degenerate bound states centred in the different wells. We call[2] $w_0(x)$ the (normalised) wavefunction of the bound state sitting in one reference well,

[2]The symbol w stands for "Wannier": see the brief introduction to Wannier functions in Sec. 1.2.

```
1  import numpy as np
2  import matplotlib.pyplot as plt
3
4  #Lattice potential is v(x)=v0*sin(kR*x)**2
5  #Unit of length: 1/kR; of momentum: kR; of energy: eR=(hbar*k)**2/(2m)
6
7  v0=5                    #Lattice energy amplitude in units of eR
8  jM=10                   #Maximum index for Fourier component
9  iM=2*jM+1               #Keep 2*jM+1 components
10 nq=101                  #Number of momentum values to consider
11 qtab=np.linspace(-1,1,num=nq) #Array containing the different momenta
12
13 enmat=np.zeros((iM,nq))   #enmat has iM lines, nq columns
14 coeffsarray=np.zeros((iM,iM,nq))   #Store eigenvectors here
15 for iq in range(nq):
16     qval=qtab[iq]
17     m=np.zeros((iM,iM))   #Truncated matrix acting on Fourier coeffs
18     for i in range(iM):   #Indices i shifted by iM to start at 0
19         m[i][i]=(2.*(i-jM)+qval)**2+.5*v0    #Diagonal matrix elements
20         if (i==0):        #First line in the matrix
21             m[i][i+1]=-.25*v0                #Element above diagonal
22         elif (i==iM-1):   #Last  line in the matrix
23             m[i][i-1]=-.25*v0                #Element below diagonal
24         else:             #Bulk       of the matrix
25             m[i][i+1]=-.25*v0                #Element above diagonal
26             m[i][i-1]=-.25*v0                #Element below diagonal
27     #Eigenvectors and eigenvalues for q=qval
28     qenergiestab,qcoeffstab=np.linalg.eigh(m)
29     #Col. iq of enmat contains iM eigvals for qtab[iq]
30     enmat[:,iq]=qenergiestab
31     #Store eigenvectors: second index sets band, third index sets q
32     coeffsarray[:,:,iq]=qcoeffstab
```

Listing 1: Python/NumPy script for the calculation of the first few energy bands of the periodic potential $V(x) = V_0 \sin^2(q_R x)$, characterising e.g. an optical lattice. The potential amplitude $V_0 = 5$ selected on l. 7 of the listing corresponds to the second line of Fig. 4.

```
33 #Plot first five bands (Fig. 4, second line, right panel)
34 plt.figure(1)
35 plt.plot(qtab,enmat[0,:],color='brown')
36 plt.plot(qtab,enmat[1,:],color='red')
37 plt.plot(qtab,enmat[2,:],color='orange')
38 plt.plot(qtab,enmat[3,:],color='green')
39 plt.plot(qtab,enmat[4,:],color='blue')
40 plt.xlim((-1,1))
41 plt.xticks(np.linspace(-1,1,num=3))
42 plt.xlabel('Position $x/a$')
43 plt.ylim((-1,30))
44 plt.yticks(np.linspace(0,30,num=4))
45 plt.ylabel('Energy $E/E_R$')
46 plt.axvline(x=0,color='lightgray',linestyle='dashed')
47 plt.show()
48
49 #Plot Fourier coefficients of Bloch functions
50 plt.figure(2)
51 plt.axvline(x=0,color='lightgray',linestyle='dashed')
52 plt.axhline(y=0,color='lightgray',linestyle='dashed')
53 plt.plot(np.arange(-jM,jM+1),coeffsarray[:,4,int((nq-1)/2)],'c-o')
54 plt.plot(np.arange(-jM,jM+1),coeffsarray[:,4,nq-1],'y-^')
55 plt.xlim((-10,10))
56 plt.xticks(np.linspace(-10,10,num=3))
57 plt.xlabel('Fourier mode index $j$ [mode $\exp(i\,j2\pi/a]$)')
58 plt.ylim((-1,1))
59 plt.yticks(np.linspace(-1,1,num=3))
60 plt.ylabel('Fourier coefficient $c_j$')
61 plt.text(-2.5,.85,'Band $b=4$',fontsize=15,color='blue')
62 plt.text(-.6,.15,'$q=0$',color='c')
63 plt.text(-6,-.6,'$q=\pi/a$', color='y')
64 plt.show()
```

Listing 2: Displaying the band energies and the Fourier coefficients of the Bloch functions using Matplotlib. The first set of instructions displays the first five energy bands (band index $b = 0$ to 4). The second set of instructions displays the calculated coefficients c_q defining three Bloch functions pertaining to the band $b = 4$: Line 53 displays the coefficients related to $q = 0$, whereas line 54 display those related to $q = \pi/a$.

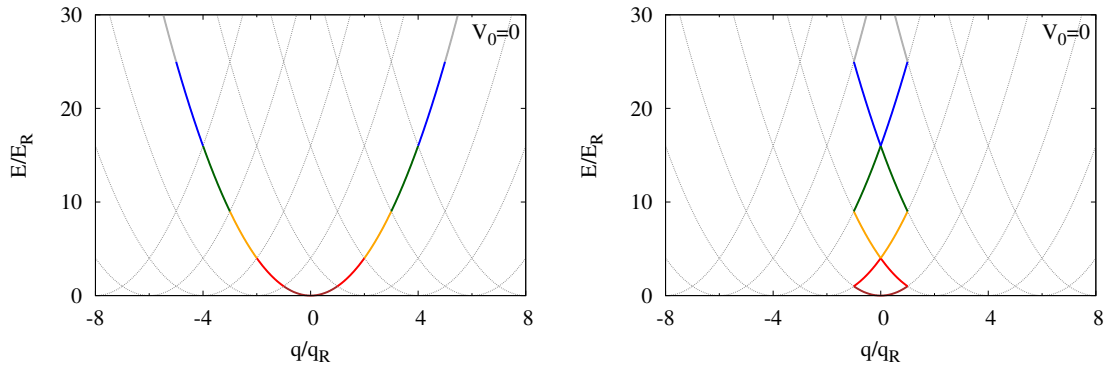

Figure 5 Dispersion relation $\epsilon(q)$ for a vanishingly small lattice amplitude $v_0 \ll \epsilon_R$. Left: It may be understood as the single parabola $\epsilon(q) = \hbar^2 q^2/(2m)$ characteristic of a single particle in free space. Then, it is defined for all wavevectors q and exhibits a single branch. Right: It may also be understood as the dispersion relation for a periodic potential of spatial period $a = \pi/q_R$. In this picture, it is defined only for wavevectors belonging to the first Brillouin zone $-q_R < q < q_R$, and it exhibits multiple branches. Each branch corresponds to a band. A weak non–vanishing lattice amplitude would lead to the opening of small energy gaps at the edges of each band ($q/q_R \approx n$ integer, where the color–code changes). On both plots, the thin dashed lines show the single–particle parabolas shifted by integer multiples of $2\pi/a = 2q_R$.

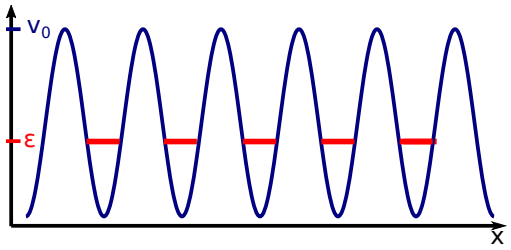

Figure 6 If the energies ϵ of all states in the band are small compared to the lattice height v_0 (bottom panels in Fig. 4), then tunnelling between the lattice sites is negligible ("atomic limit"). All sites are uncoupled. Each of them supports a bound state with the energy $\sim \epsilon$: these bound states are nearly degenerate and give rise to a nearly flat band.

which we assume to be centred on $x = 0$. The wells are evenly spaced, two consecutive wells being separated by the distance a, so that the well with index n is centred on $x = na$, and the wavefunction of the bound state in this well is $w_{0n}(x) = w_0(x - na)$. Due to the assumption that tunnelling between the wells is negligible, the wavefunctions corresponding to different wells are orthogonal, so that $\langle w_{0n}|w_{0m}\rangle = \delta_{n,m}$. The Bloch function $|\psi_{0k}\rangle$ is a linear combination of the bound–state wavefunctions $|w_{0n}\rangle$:

$$\psi_{0k}(x) \quad = \quad \sum_{n=-\infty}^{\infty} c_n \, w_0(x - na) \; , \tag{32}$$

where the complex coefficients should be chosen such that ψ_{0k} satisfies the Bloch property $\psi_{0k}(x + a) = e^{iqa}\psi_{0k}(x)$ for the quasimomentum k. Injecting this property into Eq. (32), we find:

$$\sum_{n=-\infty}^{+\infty} c_n \, w_0(x - (n-1)a) \quad = \quad e^{ika} \sum_{n=-\infty}^{+\infty} c_n \, w_0(x - na) \; . \tag{33}$$

Shifting the index of the sum on the left–hand side of Eq. (33) by one unit, and collecting the terms proportional to $w_0(x - na)$, this leads to:

$$\sum_{n=-\infty}^{+\infty} (c_{n+1} - e^{ika} c_n) \, w_0(x - na) \quad = \quad 0 \quad . \tag{34}$$

Exploiting the orthogonality of the functions $|w_{0n}\rangle$, we obtain $c_{n+1} = e^{ika} c_0$. Therefore, the Bloch function $|\psi_{nk}\rangle$ is determined up to the complex multiplicative factor $c_0 = c_{0k}$ (which could a priori

depend on the quasimomentum k):

$$\psi_{0k}(x) \quad = \quad c_{0k} \sum_{n=-\infty}^{+\infty} e^{inka}\, w_0(x-na) \ . \tag{35}$$

The corresponding band function $u_{0k}(x)$ reads:

$$u_{0k}(x) \quad = \quad \psi_{0k}(x)\, e^{-ikx} \quad = \quad c_{0k} \sum_{n=-\infty}^{+\infty} e^{-ik(x-na)}\, w_0(x-na) \ , \tag{36}$$

and it is indeed spatially periodic with the period a, as expected.

Let us calculate the overlap between two Bloch wavefunctions with the quasimomenta k and k':

$$\begin{aligned} \langle \psi_{0k} | \psi_{0k'} \rangle \quad &= \quad c_{0k}^* c_{0k'} \sum_{n=-\infty}^{+\infty} \sum_{n'=-\infty}^{+\infty} e^{-inka}\, e^{+ink'a} \int dx\, w_0^*(x-na) w_0(x-n'a) \\ &= \quad c_{0k}^* c_{0k'} \sum_{n=-\infty}^{+\infty} e^{in(k-k')a} \ , \end{aligned} \tag{37}$$

where the second step follows from the orthonormality of the bound–state wavefunctions ($|w_{0n}\rangle$). The sum of imaginary exponentials appearing in Eq. (37) is related to the "Sha function" Ш, also called 'grating function' in optics and 'Dirac comb' in signal processing, which is an infinite series of evenly–spaced Dirac peaks:

$$\text{Ш}(u) \quad = \quad \sum_{p=-\infty}^{+\infty} \delta(u-p) \quad = \quad \sum_{n=-\infty}^{+\infty} e^{i2\pi nu} \ . \tag{38}$$

The second equality in Eq. (38) is readily established by expanding the periodic "function" Ш into its Fourier series[3]. Injecting Eq. (38) into Eq. (37), we obtain:

$$\langle \psi_{0k} | \psi_{0k'} \rangle \quad = \quad c_{0k}^* c_{0k'}\, \text{Ш}\left(\frac{k-k'}{2\pi/a} \right) \ . \tag{39}$$

Eq. (39) shows that, if k and k' are not equal up to a reciprocal lattice vector (i.e. if there is no integer p such that $k' = k + p\, 2\pi/a$), then the Bloch wavefunctions $|\psi_{0k}\rangle$ and $|\psi_{0k'}\rangle$ are orthogonal, as expected. By contrast, if k and k' are equal up to a reciprocal lattice vector (i.e. if $k' = k + p\, 2\pi/a$ for some integer p), then the overlap $\langle \psi_{0k} | \psi_{0k'} \rangle$ is infinite. This is also not a surprise: in this second case, the two Bloch wavefunctions $|\psi_{0k}\rangle = |\psi_{0k'}\rangle$ coincide, so that the sought overlap is actually the squared norm of the Bloch function, $\langle \psi_{0k} | \psi_{0k} \rangle$. Just like plane waves, Bloch function are not localised: they extend over all space, so that their squared norm $\int_{-\infty}^{+\infty} dx\, |\psi_{0k}(x)|^2 = +\infty$.

A convenient way to normalise the Bloch wavefunctions (and hence to choose the value of the constant c_{0k} in Eq. (39)) is to exploit the spatial periodicity of the band function $u_{0k}(x)$. Instead of integrating over the whole x axis from $-\infty$ to $+\infty$, we integrate over a single spatial period a, say from $x = -a/2$ to $x = a/2$, and impose the condition:

$$1 \quad = \quad \int_{-a/2}^{+a/2} dx\, |\psi_{0k}(x)|^2 \quad = \quad \int_{-a/2}^{+a/2} dx\, |u_{0k}(x)|^2 \ . \tag{40}$$

Replacing Eq. (36) into Eq. (40) leads to:

$$1 \quad = \quad |c_{0k}|^2 \sum_{n=-\infty}^{+\infty} \sum_{n'=-\infty}^{+\infty} e^{ik(n'-n)a} \int_{-a/2}^{a/2} dx\, w_0^*(x-na)\, w_0(x-n'a) \ . \tag{41}$$

[3] The truncated series $D_N(u) = \sum_{n=-N}^{N} e^{i2\pi nu} = \sin[(2N+1)\pi u] / \sin(\pi u)$ approximates Ш(u) for large u. For any integer N, $D_N(u+1) = D_N(u)$ and $\int_{-1/2}^{1/2} du\, D_N(u) = 1$. It is instructive to plot $D_N(u)$ as a function of u for various values of N, and observe how the divergence for $u = 0$ (or equivalently any other integer value of u) builds up as N is increased.

The integral in the right–hand side of Eq. (41) is non–zero only if the two bound–state wavefunctions appearing there, $w_0(x - na)$ and $w_0(x - n'a)$, relate to the same well $n = n' = 0$ selected by the bounds of the integral. Hence, only the term $n = n' = 0$ survives in the double sum, and Eq. (41) reduces to $|c_{0k}|^2 = 1$. Therefore, up to an arbitrary phase, one may choose $c_{0k} = 1$. This is the normalisation convention used e.g. in Ref. [1, Sec. II.B].

1.3.2. Single–band approximation

If the temperature and the chemical potential are small enough compared to the energy spacing between the lowest–energy band (represented in brown on Fig. 4) and the next–lowest one (represented in red), then one may replace the complete Hamiltonian by an approximate, single–band Hamiltonian. In this context, the most frequently used model is the Hubbard Hamiltonian, whose second–quantised form reads:

$$H_{\text{Hubbard}} = -J \sum_{<i,j>} a_i^\dagger a_j + \frac{U}{2} \sum_i n_i(n_i - 1) \ . \tag{42}$$

The Hamiltonian H_{Hubbard} of Eq. (42) is applicable both to fermions ('Fermi–Hubbard' model) and to bosons ('Bose–Hubbard model'). It holds in any dimension and for any lattice geometry (3D cubic, 2D hexagonal, ...). The first sum, proportional to $-J$, describes the tunnelling between nearest–neighbouring lattice sites $< i, j >$. It plays an equivalent role, in this lattice model, to the kinetic energy term $p^2/(2m)$ in continuum–space models. The coefficient $J > 0$ is positive so as to ensure that it is energetically favourable for a wave packet to spread over all sites (just like kinetic energy is positive because it is energetically favourable for a wavepacket to spread throughout all space). The second term, proportional to U, describes the on–site interaction between particles in a given lattice site, whose number (which is not necessarily fixed) is given by the number operator $n_i = a_i^\dagger a_i$ related to the site i. The coefficient U is positive for repulsive interactions (in which case the presence of multiple particles within the same lattice site is energetically disfavoured) and negative for attractive interactions (in which case the presence of multiple particles on the same site is energetically favoured). The Hubbard model neglects interactions between particles in different sites, hence, it is applicable in the case where the interaction between two particles has a range which is shorter than the lattice spacing. In particular, it holds for neutral cold atoms, whose interactions are often short–ranged. In the presence of longer–ranged interactions (Coulomb interactions for ions, dipole–dipole interactions for atoms or molecules carrying a magnetic or electric dipole moment, Rydberg atoms ...), the Hubbard model of Eq. (42) is no longer directly applicable, but it may be generalised to account e.g. for nearest–neighbour interactions.

We have already encountered the first–quantised version of the Hubbard Hamiltonian (Eq. (5) above). We shall study many of these properties in the context of this problem. In particular, we shall analyse its band structure, and show that it supports only a single band, in Sec. 2.1.

2. Question 5: single–particle energy spectrum, superfluid state

In this question, we totally neglect on–site interactions: $U = 0$. Therefore, we are dealing with a system of non–interacting particles governed by the following lattice Hamiltonian:

$$H = -J \sum_{<i,j>} a_i^\dagger a_j \ , \tag{43}$$

where $J > 0$ is the tunnelling amplitude between nearest neighbours $< i, j >$.

In order to construct the many–particle ground state for this non–interacting system, we follow the following two–step procedure: *(i)* We determine the single–particle eigenstates and energies; *(ii)* We combine single–particle states so as to satisfy the considered quantum statistics.

2.1. Single–particle eigenstates and energies for the Bose–Hubbard model

For simplicity, we focus on the case of a one–dimensional (1D) lattice, but the two– and three–dimensional cases are very similar. In the 1D case, the discrete lattice sites are at the positions $x_n = na$, where n is an integer such that $1 \leq n \leq N_l$ and N_l is the total number of lattice sites. We represent these N_l sites by the kets $|n\rangle$. We use periodic boundary conditions, i.e. $|0\rangle = |N_l\rangle$ and $|N_l + 1\rangle = |1\rangle$. Under these conditions, each lattice site $|n\rangle$ has two nearest neighbours which are $|n-1\rangle$ and $|n+1\rangle$, so that the single–particle Hamiltonian associated with Eq. 43 is:

$$h = -J \sum_{n=1}^{N_l} \left(|n-1\rangle \langle n| + |n+1\rangle \langle n| \right) . \tag{44}$$

The single–particle Hamiltonian is spatially periodic, therefore we seek single–particle eigenstates in the form of Bloch waves $\psi_{k,b}(x)$, defined by:

$$\psi_{k,b}(x) = e^{ikx}\, u_{k,b}(x) , \tag{45}$$

where e^{ikx} is a plane wave and $u_{k,b}(x)$ is a spatially–periodic function whose period coincides with that of the lattice, and which depends both on k and on a discrete index b. The quantity k appearing in the plane wave is called the *quasimomentum* or *crystal momentum*; the choice of the index b labelling $u_{\boldsymbol{k},b}$ defines the *band*.

For the lattice Hamiltonian of Eq. 44, the wavefunctions $\psi_{k,b}(x)$, and hence the functions $u_{k,b}$ and e^{ikx}, are defined at the discrete spatial points $x_n = na$ corresponding to the lattice sites $|n\rangle$. A suitable band function $u_{k,b}$ must have the same spatial period as that of the Hamiltonian, meaning that $u_{k,b}(na) = u_{k,b}((n+1)a)$, so that $u_{k,b}$ must be constant. Therefore, the Hubbard model supports only one band, a characteristic property which it is useful to keep in mind.

Because the band function $u_{k,b}$ is constant, the Bloch waves $\psi_{k,b}$ reduce to $\psi_k(x_n) = e^{inka}/\sqrt{N_l}$, where the prefactor $1/\sqrt{N_l}$ has been chosen to ensure the normalisation $\langle \psi_k | \psi_k \rangle = 1$. This may be written in terms of kets:

$$|\psi_k\rangle = \frac{1}{\sqrt{N_l}} \sum_{n=1}^{N_l} e^{inka} |n\rangle \ . \tag{46}$$

Acting with h on $|\psi_k\rangle$, one obtains:

$$h|\psi_k\rangle = -J \sum_n (|n-1\rangle \langle n| + |n+1\rangle \langle n|) \frac{1}{\sqrt{N_l}} \sum_m e^{imka} |m\rangle \tag{47}$$

$$= -\frac{J}{\sqrt{N_l}} \sum_n e^{inka} (|n-1\rangle + |n+1\rangle) \tag{48}$$

$$= -Je^{ika} \left(\frac{1}{\sqrt{N_l}} \sum_n e^{i(n-1)ka} |n-1\rangle \right) - Je^{-ika} \left(\frac{1}{\sqrt{N_l}} \sum_n e^{i(n+1)ka} |n+1\rangle \right) . \tag{49}$$

Thanks to the periodic boundary conditions, we replace each of the two sums in Eq. 49 by $|\psi_k\rangle$:

$$h|\psi_k\rangle = -J(e^{ika} + e^{-ika}) |\psi_k\rangle = -2J\cos(ka) |\psi_k\rangle \ , \tag{50}$$

which shows that $|\psi_k\rangle$ is an eigenstate of h corresponding to the eigenvalue $\epsilon_k = -2J\cos(ka)$.

The plane wave $|\psi_k\rangle$, considered as a continuum–space function rather than just sampled on the lattice sites, would also be an eigenstate of the Hamiltonian $p^2/(2m)$ representing a single particle in free space. However, the periodicity of the lattice transforms the quadratic free–space dispersion relation $\epsilon(k) = \hbar^2 k^2/(2m)$ into the sinusoidal dependence $\epsilon_k = -2J\cos(ka)$.

Which are the allowed independent values of k?

The relevant set of values of $\boldsymbol{k}$ is constrainted by two different phenomena.

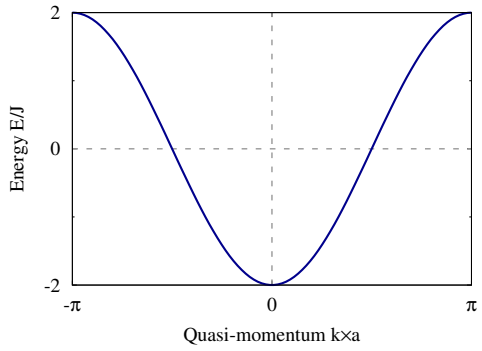

Figure 7 Single–particle energy spectrum for the Hubbard model of Eq. 44.

First, the periodic boundary conditions require that $e^{iN_l ka} = 1$. This means that the allowed wavectors k may be labelled with an integer index p such that:

$$k_p = \frac{p}{N_l}\frac{2\pi}{a} \ . \tag{51}$$

For an infinite chain $N_l \to \infty$, we recover a continuum of allowed values for k.

The second property, which is characteristic of periodic Hamiltonians, reduces the set of independent values of k. The Bloch wave of Eq. 45 satisfies[4]:

$$\psi_{k,b}(x+a) = e^{ika}\,\psi_{k,b}(x) \ . \tag{52}$$

Equation 52, which is a concise but complete statement of Bloch's theorem, fully characterises the Bloch wave $\psi_{k,b}(x)$. The wavevector k only appears in the phase factor e^{ika}, hence, values of k which differ by an integer multiple of $2\pi/a$ play exactly the same role. Therefore, in order to describe all available single–particle states, it is sufficient to restrict the values of k to an interval of length $2\pi/a$, called "first Brillouin zone". It is because of this second constraint on the independent values of $\boldsymbol{k}$ that, in the context of periodic lattice models, this quantity is called "quasimomentum" rather than just momentum.

The energy spectrum of Eq. 50 is represented on Fig. 7. The ground–state, corresponding to $k = 0$, has the energy $\epsilon_0 = -2J$ and is non–degenerate. The maximum–energy state, corresponding to $k = \pi$ and the energy $\epsilon_\pi = +2J$, is also non–degenerate because the first Brillouin zone contains either $k = \pi/a$ or $k = -\pi/a$ (the choice has no consequence), but not both. However, all other states are twice degenerate: $\epsilon_k = \epsilon_{-k}$, because the Hubbard Hamiltonian of Eq. 44 is invariant under the parity operation (which maps $|k\rangle$ onto $|-k\rangle$).

2.2. Many–particle ground state for bosons

For identical bosons, the many–particle ground state is obtained by choosing all atoms to be in the single–particle ground state:

$$|\psi_{\boldsymbol{k}=\boldsymbol{0}}\rangle = \frac{1}{\sqrt{N_l}}\sum_{n=0}^{N_l}|n\rangle \ . \tag{53}$$

There is no limit to the number N_a of bosons that may be accommodated by this ground state.

Remembering that creation operators transform like kets, Eq. (53) may be used to express the operator $a^\dagger_{\boldsymbol{k}=\boldsymbol{0}}$ in terms of the creation operators on single sites $a^\dagger_n$:

$$a^\dagger_{\boldsymbol{k}=\boldsymbol{0}} = \frac{1}{\sqrt{N_l}}\sum_{n=0}^{N_l} a^\dagger_n \ . \tag{54}$$

[4]To derive Eq. (52) from Eq. (45), write $\psi_{k,b}(x+a) = e^{ik(x+a)}\,u_{k,b}(x+a) = e^{ika}e^{ikx}\,u_{k,b}(x) = e^{ika}\,\psi_{k,b}(x)$. In order to check the equivalence of Eq. (52) with Bloch's theorem, consider $u_{k,b}(x) = e^{-ikx}\psi_{k,b}(x)$.

Therefore, the ground state for N_a identical bosons is:

$$|\mathrm{SF}_{N_a}\rangle = \frac{1}{\sqrt{N_a!}}\, a_{\boldsymbol{k}=\boldsymbol{0}}^{\dagger N_a}\,|\mathrm{vac}\rangle = \frac{1}{\sqrt{N_a!}}\left(\frac{1}{\sqrt{N_l}}\sum_i a_i^\dagger\right)^{N_a}|\mathrm{vac}\rangle \ . \tag{55}$$

2.3. Many–particle ground state for fermions

[This paragraph is an addendum which does not correspond to a question in the problem set.]

For identical fermions, we must construct a Fermi sea using the single–particle states $|\psi_k\rangle$.

If the lattice contains N_l lattice sites, then there are N_l independent single–particle states, hence, the atom number must satisfy $N_a \leq N_l$.

We order the single–particle states $(|\psi_j\rangle)_{0\leq j\leq N_l-1}$ by increasing energies:

$$\epsilon_0 < \quad \epsilon_1 = \epsilon_2 \quad < \ldots < \quad \epsilon_{N_l-3} = \epsilon_{N_l-2} \quad < \epsilon_{N_l-1} \ , \tag{56}$$

where we have made the degeneracies $\epsilon_k = \epsilon_{-k}$ explicit. We introduce the corresponding creation operators $(a_j^\dagger)_{0\leq j\leq N_l}$, which may be expressed in terms of the operators $a_n^\dagger$ (each of which creates a fermion in the site n) using Eq. (46). Then, the fermionic ground state for N_a atoms reads:

$$|\Psi_{N_a}\rangle = a_0^\dagger a_1^\dagger \cdots a_{N_a}^\dagger\,|\mathrm{vac}\rangle \ . \tag{57}$$

If N_a is even, with $2 \leq N_a \leq N_l - 2$, the ground state is two–fold degenerate. This is because the highest–energy populated level may correspond to either $|\psi_{+k_F}\rangle$ or $|\psi_{-k_F}\rangle$, in accordance with the invariance of the many–body Hamiltonian under the parity operation.

3. Question 6: one–body density matrix in the superfluid regime

3.1. Explicit expression for the superfluid state

In Eq. 55, N_l is the total number of sites in the lattice. The operator $a_i^\dagger$ creates an atom in the lattice site $|i\rangle$, whereas $a_{\boldsymbol{k}=\boldsymbol{0}}^\dagger$ creates an atom in the single–particle ground state $|\boldsymbol{k}=\boldsymbol{0}\rangle = \sum_i |i\rangle / \sqrt{N_l}$. Equation 55 simply expresses the fact that all atoms are in the ground state $|\boldsymbol{k}=\boldsymbol{0}\rangle$.

First, we expand the parentheses on the right–hand side of Eq. 55 using the multinomial formula:

$$|\mathrm{SF}_{N_a}\rangle = \frac{1}{\sqrt{N_a!}}\,\frac{1}{N_l^{N_a/2}}\sum_{n_1+\cdots+n_{N_l}=N_a}\frac{N_a!}{n_1!\cdots n_{N_l}!}\,a_1^{\dagger n_1}\cdots a_{N_l}^{\dagger n_{N_l}}\,|\mathrm{vac}\rangle \ . \tag{58}$$

Then, we act on $|\mathrm{vac}\rangle$ using the $a_i^\dagger$, accounting for the normalisation factors $a_i^{\dagger n_i}\,|\mathrm{vac}\rangle = \sqrt{n_i!}\,|n_i\rangle$:

$$|\mathrm{SF}_{N_a}\rangle = \frac{1}{N_l^{N_a/2}}\sum_{n_1+\cdots+n_{N_l}=N_a}\left(\frac{N_a!}{n_1!\cdots n_{N_l}!}\right)^{1/2}|n_1,\ldots,n_{N_l}\rangle \ , \tag{59}$$

where the ket $|n_1,\ldots,n_{N_l}\rangle$ is the N_a–particle state where site 1 contains n_1 particles, …, and site N_l contains n_{N_l} atoms.

3.2. Annihilating a particle in the superfluid state

Now, we act on the N_a–particle state $|\mathrm{SF}_{N_a}\rangle$ using the annihilation operator a_j, which destroys a particle on the lattice site i. This calculation may be carried out starting from the explicit expression for $|\mathrm{SF}_{N_a}\rangle$ given by Eq. (59) (see Sec. 3.2.1). The result may also be established in terms of commutators (see Sec. 3.2.2 below).

3.2.1. First method, starting from the explicit expression of the superfluid state

Here, we start from Eq. (59). Recalling that $a_j \left|n_j\right\rangle = \sqrt{n_j}\left|n_j - 1\right\rangle$, we obtain:

$$a_j \left|\mathrm{SF}_{N_a}\right\rangle = \frac{1}{N_l^{N_a/2}} \sum_{n_1+\cdots+n_{N_l}=N_a} \left(\frac{N_a!}{n_1!\cdots n_{N_l}!}\right)^{1/2} \sqrt{n_j}\ \left|n_1,\ldots,n_j-1,\ldots,n_{N_l}\right\rangle\ . \tag{60}$$

Inside the parentheses on the right–hand side, we use $N_a! = N_a(N_a-1)!$ in the numerator and $n_i! = n_i(n_i-1)!$ in the denominator. We also write $N_l^{N_a/2} = \sqrt{N_l} N_l^{(N_a-1)/2}$. This leads to:

$$a_j \left|\mathrm{SF}_{N_a}\right\rangle = \sqrt{\frac{N_a}{N_l}} \sum_{n_1+\cdots+n_{N_l}=N_a} \left(\frac{(N_a-1)!}{n_1!\cdots(n_j-1)!\cdots n_{N_l}!}\right)^{1/2} \left|n_1,\ldots,n_j-1,\ldots,n_{N_l}\right\rangle\ . \tag{61}$$

Now, we inspect the N_l–uplets $(n_1,\ldots,n_{N_l})$ over which the sum in Eq. 61 is performed. We retain those N_l–uplets for which:

$$n_1+\cdots+n_j+\cdots+n_{N_l} = N_a, \quad \text{that is,} \quad n_1+\cdots+(n_j-1)+\cdots+n_{N_l} = N_a-1\ . \tag{62}$$

The second form of the condition of Eq. 62 is inapplicable to the N_l–uplets for which $n_j = 0$; however, these terms do not contribute to the sum because then $a_j \left|n_j = 0\right\rangle = 0$. Therefore, Eq. 61 may be rewritten as:

$$a_j \left|\mathrm{SF}_{N_a}\right\rangle = \sqrt{\frac{N_a}{N_l}} \sum_{n_1+\cdots+(n_j-1)+\cdots+n_{N_l}=N_a} \left(\frac{(N_a-1)!}{n_1!\cdots(n_j-1)!\cdots n_{N_l}!}\right)^{1/2} \left|n_1,\ldots,n_j-1,\ldots,n_{N_l}\right\rangle\ . \tag{63}$$

We change variables from $n_j \geq 1$ to $\tilde{n_j} = n_j - 1 \geq 0$. We then recognise on the right–hand side, up to a numerical prefactor, the superfluid state $\left|\mathrm{SF}_{N_a-1}\right\rangle$ which contains (N_a-1) atoms. Hence:

$$a_j \left|\mathrm{SF}_{N_a}\right\rangle = \sqrt{\frac{N_a}{N_l}}\ \left|\mathrm{SF}_{N_a-1}\right\rangle\ . \tag{64}$$

Note that $a_j \left|\mathrm{SF}_{N_a}\right\rangle$ does not depend on the site j in which the particle is annihilated.

3.2.2. Second method, using commutators

The action of the annihilation operator a_j for any site j on the superfluid state $\left|\mathrm{SF}_{N_a}\right\rangle$, summarised by Eq. (64), may be established without using the explicit expression for $\left|\mathrm{SF}_{N_a}\right\rangle$ given by Eq. (59).

Instead, we start from the following relation involving the commutator $[a_j, a_{\boldsymbol{k}=\boldsymbol{0}}^{\dagger N_A}]$:

$$a_j \left|\mathrm{SF}_{N_a}\right\rangle = a_j \frac{1}{\sqrt{N_a!}} a_{\boldsymbol{k}=\boldsymbol{0}}^{\dagger N_a} \left|\mathrm{vac}\right\rangle \quad = \frac{1}{\sqrt{N_a!}} \left([a_j, a_{\boldsymbol{k}=\boldsymbol{0}}^{\dagger N_A}] + a_{\boldsymbol{k}=\boldsymbol{0}}^{\dagger N_A} a_j\right) \left|\mathrm{vac}\right\rangle \quad = \frac{1}{\sqrt{N_a!}} [a_j, a_{\boldsymbol{k}=\boldsymbol{0}}^{\dagger N_A}] \left|\mathrm{vac}\right\rangle\ . \tag{65}$$

In Eq. (64), the first step follows from Eq. (55), and the last one reflects $a_j \left|\mathrm{vac}\right\rangle = 0$.

Thanks to Eq. (64), the calculation of $a_j \left|\mathrm{SF}_{N_a}\right\rangle$ now hinges on the evaluation of the commutators $[a_j, a_{\boldsymbol{k}=\boldsymbol{0}}^{\dagger p}]$, where p is a positive integer. Starting from Eq. (54), we first obtain:

$$[a_j, a_{\boldsymbol{k}=\boldsymbol{0}}^{\dagger}] = \frac{1}{\sqrt{N_l}}\ . \tag{66}$$

Next, we recall the property $[A, BC] = [A, B]C + B[A, C]$ stating that commutators $[A, \cdot]$ behave like derivatives. Hence:

$$[a_j, a_{\boldsymbol{k}=\boldsymbol{0}}^{\dagger 2}] = [a_j, a_{\boldsymbol{k}=\boldsymbol{0}}^{\dagger}]\ a_{\boldsymbol{k}=\boldsymbol{0}}^{\dagger} + a_{\boldsymbol{k}=\boldsymbol{0}}^{\dagger}\ [a_j, a_{\boldsymbol{k}=\boldsymbol{0}}^{\dagger}] \quad = \frac{2}{\sqrt{N_l}}\, a_j\ , \tag{67}$$

where the second step relies on Eq. (66). Similarly:

$$[a_j, a^{\dagger 3}_{\boldsymbol{k}=\boldsymbol{0}}] = [a_j, a^{\dagger 2}_{\boldsymbol{k}=\boldsymbol{0}}]\, a^{\dagger}_{\boldsymbol{k}=\boldsymbol{0}} + a^{\dagger}_{\boldsymbol{k}=\boldsymbol{0}}\, [a_j, a^{\dagger 2}_{\boldsymbol{k}=\boldsymbol{0}}] \quad = \frac{2}{\sqrt{N_l}}\, a^{\dagger 2}_{\boldsymbol{k}=\boldsymbol{0}} + a^{\dagger 2}_{\boldsymbol{k}=\boldsymbol{0}} \frac{1}{\sqrt{N_l}} \quad = \frac{3}{\sqrt{N_l}}\, a^{\dagger 2}_{\boldsymbol{k}=\boldsymbol{0}} \ , \quad (68)$$

where we have used both Eq. (66) and (67). An immediate recursion then yields:

$$[a_j, a^{\dagger p}_{\boldsymbol{k}=\boldsymbol{0}}] = \frac{p}{\sqrt{N_l}}\, a^{\dagger (p-1)}_{\boldsymbol{k}=\boldsymbol{0}} \quad \text{for any integer } p \geq 0. \ . \quad (69)$$

Injecting Eq. (69), applied for $p = N_a$, into the last step of Eq. (65), we conclude:

$$a_j\, |\mathrm{SF}_{N_a}\rangle = \frac{1}{\sqrt{N_a!}} \frac{N_a}{\sqrt{N_l}} a^{\dagger (N_a-1)}_{\boldsymbol{k}=\boldsymbol{0}}\, |\mathrm{vac}\rangle \quad = \sqrt{\frac{N_a}{N_l}} \frac{1}{\sqrt{(N_a-1)!}} a^{\dagger (N_a-1)}_{\boldsymbol{k}=\boldsymbol{0}}\, |\mathrm{vac}\rangle \quad = \sqrt{\frac{N_a}{N_l}}\, |\mathrm{SF}_{N_a-1}\rangle \ , \quad (70)$$

where the final result coincides with Eq. (64), as expected.

3.2.3. Thermodynamic limit: approximate site–wise factorisation of the superfluid state

Thermodynamic limit. In this limit, both the number of atoms, N_a, and the number of sites, N_l, are sent to infinity (experimentally speaking, they are chosen to be very large), but with the constraint that the filling factor $\nu = N_a/N_l$ should remain constant. This limit leads to a number of simplifications. In particular, the result $a_j^2\, |\mathrm{SF}_{N_a}\rangle = [N_a(N_a-1)]^{1/2}/N_l\ |\mathrm{SF}_{N_a-2}\rangle$, which holds regardless of the value of N_a, reduces to $a_j^2\, |\mathrm{SF}_{N_a}\rangle = \nu\, |\mathrm{SF}_{N_a-2}\rangle$ in the thermodynamic limit. Combining this result with Eq. (64), and using the bosonic commutation relation $a_j^\dagger a_j = a_j a_j^\dagger - 1$, we conclude that, in the superfluid state $|\mathrm{SF}_{N_a}\rangle$, the average number of atoms on site j, $\langle n_j\rangle = \langle \mathrm{SF}_{N_a}|n_j|\mathrm{SF}_{N_a}\rangle$, is equal to the variance $\Delta n_j^2 = \langle \mathrm{SF}_{N_a}|n_j^2|\mathrm{SF}_{N_a}\rangle - \langle n_j\rangle^2$ of this atom number:

$$\text{In the thermodynamic limit,} \quad \langle n_j\rangle \quad = \quad \Delta n_j^2 \quad = \quad \nu \ . \quad (71)$$

Equation (71) suggests that the statistical distribution of the atom number n_i on a given site, calculated in the many–particle state $|\mathrm{SF}_{N_a}\rangle$, may be expected to be Poissonian.

Site–wise factorised state $|\Psi_{\mathrm{coh}}\rangle$. The intuition behind the approximation introduced in this section is that, in the thermodynamic limit, the superfluid states $|\mathrm{SF}_{N_a}\rangle$ and $|\mathrm{SF}_{N_a-1}\rangle$, respectively comprised of N_a and $N_a - 1$ atoms, should be very similar. Then, Eq. (64) indicates that $|\mathrm{SF}_{N_a}\rangle$ is an approximate eigenstate of the annihilation operator a_j corresponding to the eigenvalue $\sqrt{\nu}$. Therefore, we shall compare $|\mathrm{SF}_{N_a}\rangle$ to the state $|\Psi_{\mathrm{coh}}\rangle$ defined as follows:

$$|\Psi_{\mathrm{coh}}\rangle \quad = \quad \bigotimes_{j=1}^{N_l} |\sqrt{\nu}^{(j)}\rangle \ , \quad (72)$$

with $|\sqrt{\nu}^{(j)}\rangle$ being the coherent state[5] for the site j such that $a_j\, |\sqrt{\nu}^{(j)}\rangle = \sqrt{\nu}\, |\sqrt{\nu}^{(j)}\rangle$. The state $|\Psi_{\mathrm{coh}}\rangle$ exhibits three important properties:

1. It is factorised as a tensor product of wavefunctions each corresponding to a given site (j);
2. All sites are represented by the same single–site wavefunction $|sqrt\nu^{(j)}\rangle$;
3. Unlike for $|\mathrm{SF}_{N_a}\rangle$, whose total number of atoms is well–defined (equal to N_a), the state $|\Psi_{\mathrm{coh}}\rangle$ is not an eigenstate of the operator $n_1 + \cdots + n_{N_l}$, i.e. the total atom number fluctuates.

[5] Coherent states and their most important properties are briefly reviewed in Appendix A of these notes.

Explicit expression for $|\Psi_{\rm coh}\rangle$. In Eq. (72), we replace the coherent state $|\sqrt{\nu}^{(j)}\rangle$ by its explicit expression given by Eq. (126), and then expand the tensor product:

$$\begin{aligned} |\Psi_{\rm coh}\rangle &= \bigotimes_{j=1}^{N_l} \left[e^{-\nu/2} \sum_{n_j=0}^{+\infty} \left(\frac{\nu^{n_j}}{n_j!} \right)^{1/2} |n^{(j)}\rangle \right] \\ &= e^{-N_l\nu/2} \sum_{n_1=0}^{+\infty} \cdots \sum_{n_{N_l}=0}^{+\infty} \left(\frac{\nu^{n_1+\cdots+n_{N_l}}}{n_1!\cdots n_{N_l}!} \right)^{(1/2)} |n_1 \ldots n_{N_l}\rangle \ . \end{aligned} \tag{73}$$

In Eq. (73), we replace the filling fraction ν by its expression $\nu = N_a/N_l$. Furthermore, the presence of the term $\nu^{n_1+\cdots+n_{N_l}}$ suggests that it is favourable to reorganise the multiple sums on the atom numbers $n_1, \ldots, n_{N_l}$ in the following way: First, we fix the total atom number N; then, we choose the positive values of $n_1, \ldots, n_{N_l}$ such that $n_1 + \cdots + n_{N_l} = N$. This leads to:

$$|\Psi_{\rm coh}\rangle = \sum_{N=0}^{+\infty} \left(e^{-N_a} \frac{N_a^N}{N!} \right)^{1/2} \sum_{n_1+\cdots+n_{N_l}=N} \left(\frac{1}{N_l^N} \frac{N!}{n_1!\cdots n_{N_l}!} \right)^{1/2} |n_1 \ldots n_{N_l}\rangle \ , \tag{74}$$

In Eq. (74), we recognise that the inner sum (taken on the atom numbers $n_j \geq 0$ such that $n_1 + \cdots + n_{N_l} = N$) matches the explicit expression for $|{\rm SF}_N\rangle$ given by Eq. (59). Hence,

$$|\Psi_{\rm coh}\rangle = \sum_{N=0}^{+\infty} \left(e^{-N_a} \frac{N_a^N}{N!} \right)^{1/2} |{\rm SF}_N\rangle \ . \tag{75}$$

The state $|\Psi_{\rm coh}\rangle$ is actually a coherent state of the annihilation operator $a_{\boldsymbol{k}=0}$ (see also questions 15 and 16 of the problem set, and their solution in Sec. 6 of the present notes). To establish this result, we replace $|{\rm SF}_N\rangle$ in Eq. (75) by its expression in terms of $a_{\boldsymbol{k}=\boldsymbol{0}}^{\dagger N}|{\rm vac}\rangle$ given by Eq. (55):

$$|\Psi_{\rm coh}\rangle = e^{-N_a/2} \sum_{N=0}^{+\infty} \frac{1}{N!} (\sqrt{N_a} a_{\boldsymbol{k}=\boldsymbol{0}}^{\dagger})^N |{\rm vac}\rangle = e^{-N_a/2} \exp\left(\sqrt{N_a}\, a_{\boldsymbol{k}=\boldsymbol{0}}^{\dagger} \right) |{\rm vac}\rangle \ , \tag{76}$$

where the second step follows from the definition of the exponential of the operator $\sqrt{N_a}\, a_{\boldsymbol{k}=\boldsymbol{0}}^{\dagger}$. Finally, Eq. (126) in the appendix allows us to conclude.

Discussion of the state $|\Psi_{\rm coh}\rangle$. Let us summarise Eqs. (72) and (75) above in a single equation:

$$|\Psi_{\rm coh}\rangle = \bigotimes_{j=1}^{N_l} |\sqrt{\nu}^{(j)}\rangle = \sum_{N=0}^{+\infty} \left(e^{-N_a} \frac{N_a^N}{N!} \right)^{1/2} |{\rm SF}_N\rangle \ . \tag{77}$$

The state $|\Psi_{\rm coh}\rangle$ is a linear superposition of the superfluid states[6] $|{\rm SF}_N\rangle$ for all possible values of the total particle number N, reflecting the fact that, in in this state, the total particle number is not conserved. The probability p_N for finding N particles in the system may be read directly off the right–hand side of Eq. (77): it is the square of the amplitude of the component along $|{\rm SF}_N\rangle$, that is to say, $p_N = e^{-N_a}\, N_a^N/N!$. This is a Poisson distribution, so that the mean value $\langle N\rangle$ of the total atom number and its variance ΔN^2 are equal: $\langle N\rangle = \Delta N^2 = N_a$. Thus, the standard deviation ΔN satisfies $\Delta N/\langle N\rangle = 1/\sqrt{N_a}$.

In the thermodynamic limit, N_a is very large, hence, $\Delta N/\langle N\rangle$ is very small. This means that the fluctuations on the total atom number N are neglibible, and the distribution is strongly peaked

[6] For two different atom numbers $N \neq N'$, the states $|{\rm SF}_N\rangle$ and $|{\rm SF}_{N'}\rangle$ are orthogonal. This follows from their being eigenvectors of the *hermitian* operator $\hat{N}$ giving the total atom number, for different eigenvalues. Indeed, $\hat{N}\,|{\rm SF}_N\rangle = N\,|{\rm SF}_N\rangle$ and $\langle {\rm SF}_{N'}|\,\hat{N} = N'\,\langle {\rm SF}_{N'}|$ (the property involving bras relies on the hermiticity of $\hat{N}$). Hence, $\langle {\rm SF}_{N'}|\hat{N}|{\rm SF}_N\rangle = N\,\langle {\rm SF}_{N'}|{\rm SF}_N\rangle = N'\,\langle {\rm SF}_{N'}|{\rm SF}_N\rangle$, so that $(N'-N)\,\langle {\rm SF}_{N'}|{\rm SF}_N\rangle = 0$.

around its mean value N_a. Therefore, the coherent state $|\Psi_{\rm coh}\rangle$ is a very good approximation for the superfluid state $|{\rm SF}_{N_a}\rangle$. It offers a number of advantages compared to the exact superfluid state. In particular, its expression in terms of a product of coherent states on each site (first equality of Eq. (77)) shows that the probability distribution for the atom number on a given site is indeed Poissonian, as conjectured above at the beginning of Sec. 3.2.3.

Replacing a quantum state with a fixed number of particles with another state whose particle number presents small fluctuations is analogous to going, in statistical physics, from the canonical ensemble, where the particle number is rigorously fixed, to the grand–canonical ensemble, where the particle number fluctuates around its average value set by the chemical potential. This type of reasoning is ubiquitous. The most famous example is the derivation of the Bose–Einstein and Fermi–Dirac quantum statistics in the grand–canonical ensemble, discussed in Problem 2. We shall see an illustration of its usefulness in this problem, in the context of the collapse–and–revival phenomenon (see Sec. 6 below). It is also an important step in the Bardeen–Cooper–Schrieffer theory for the superfluidity of spin–balanced Fermi gases [3, §4.3].

3.3. Calculation of the one–body density matrix

In the present discrete case, the one–body density matrix is defined as:

$$\rho^{(1)}(i,j) = \langle {\rm SF}|a_i^\dagger a_j|{\rm SF}\rangle \ . \tag{78}$$

For a given pair of sites i and j, we use Eq. 64 to evaluate both $a_j\,|{\rm SF}\rangle$ and $\langle {\rm SF}|\,a_i^\dagger = (a_i\,|{\rm SF}\rangle)^\dagger$. We thus find:

$$\rho^{(1)}(i,j) = \frac{N_a}{N_l}\,\langle {\rm SF}_{N_a-1}|{\rm SF}_{N_a-1}\rangle = \nu \ , \tag{79}$$

where we have introduced the filling factor $\nu = N_a/N_l$. Equation 79 holds for all i and j, including $i=j$. The fact that $\rho^{(1)}$ is equal to a constant for large $|i-j|$ signals the presence of off–diagonal long–range order, i.e. of a Bose–Einstein condensate.

4. Quests. 10–12: mean–field description of the phase transition

We consider the full Bose–Hubbard Hamiltonian:

$$H = -J\sum_{<i,j>} a_i^\dagger a_j + \frac{U}{2}\sum_i n_i(n_i-1) \ . \tag{80}$$

The term proportional to J describes hopping between nearest–neighbouring sites $< i,j >$; the term proportional to U represents the on–site interaction.

We apply the variational principle and, hence, restrict our analysis to the following family of trial wavefunctions, where the state $|\Psi_{\theta,\phi}\rangle$ characterising the whole lattice factorises into a tensor product of single–site states $|\chi_i\rangle$ which are the same for all sites (Hartree–type ansatz):

$$|\Psi_{\theta,\phi}\rangle = \bigotimes_{i=1}^{N_l} |\chi^{(i)}_{\theta,\phi}\rangle \quad \text{where} \quad |\chi^{(i)}_{\theta,\phi}\rangle = \cos\theta\,|1\rangle + \sin\theta\,\frac{e^{-i\phi}\,|0\rangle + e^{i\phi}\,|2\rangle}{\sqrt{2}} \ . \tag{81}$$

4.1. Order parameter and identification of the two phases

The order parameter in the site i is defined as the complex number ψ_i given by the average of the annihilation operator a_i:

$$\psi_i = \langle \Psi_{\theta,\phi}|a_i|\Psi_{\theta,\phi}\rangle = \langle \chi^{(i)}|a_i|\chi^{(i)}\rangle \ , \tag{82}$$

where the second equality follows from the site–factorised form of Eq. 81. Furthermore, all lattice sites are in the same state $|\chi\rangle$, so that $\psi = \psi_i$ does not depend on the lattice site i. We first calculate $a_j\,|\chi^{(j)}\rangle = \cos\theta\,|0\rangle + e^{i\phi}\sin\theta\,|1\rangle$, and then obtain:

$$\psi = \frac{1}{2}\left(1 + \frac{1}{\sqrt{2}}\right)\sin(2\theta)e^{i\phi}\ . \tag{83}$$

For $\theta = 0$ (and arbitrary ϕ), $|\Psi_{0,\phi}\rangle = |\mathrm{MI}\rangle$, and $\psi = 0$, signalling that the Mott–insulating phase exhibits no coherence. The absence of coherence can be understood from the fact that the atom number is well–defined in each site (we have chosen it equal to 1).

On the contrary, for $0 < \theta < \pi/2$, $\psi \neq 0$, meaning that the system does exhibit coherence. All of these states constitute the superfluid phase. The modulus $|\psi_i|$ of the order parameter ψ is maximal for $\theta = \pi/4$, hence, the states $|\Psi_{\pi/4,\phi}\rangle$ may be identified as the deep superfluid state $|\mathrm{SF}\rangle$ in the mean–field approximation.

4.2. One–body density matrix

Thanks to the site–factorised form of Eq. 81, the one–body density matrix reduces to:

$$\langle\Psi_{\theta,\phi}|a_i^\dagger a_j|\Psi_{\theta,\phi}\rangle = \langle\chi^{(i)}\chi^{(j)}|a_i^\dagger a_j|\chi^{(i)}\chi^{(j)}\rangle = \langle\chi^{(i)}|a_i^\dagger|\chi^{(i)}\rangle\,\langle\chi^{(i)}|a_j|\chi^{(i)}\rangle = \psi_i^*\psi_j = |\psi|^2\ , \tag{84}$$

where we have used Eq. 82 defining $\psi_i = \psi$. We replace ψ by its expression (Eq. 83) and obtain the following result for the density matrix $\rho_{\mathrm{MF}}^{(i,j)}$ in the mean–field (MF) approximation:

$$\rho_{\mathrm{MF}}^{(i,j)} = \langle\Psi_{\theta,\phi}|a_i^\dagger a_j|\Psi_{\theta,\phi}\rangle = \frac{1}{4}\left(\frac{3}{2} + \sqrt{2}\right)\sin^2(2\theta)\ . \tag{85}$$

Note that $\rho_{\mathrm{MF}}^{(i,j)}$ vanishes in the Mott–Insulator phase ($\theta = 0$), and non–zero for any $0 < \theta < \pi$, in which case it is independent of the lattice sites i, j. In particular, the system does exhibit off–diagonal long–range order in the superfluid phase.

4.3. Contribution of the hopping term

The mean value of the hopping term is related to the uniform value of the off–diagonal density matrix. We call z the number of nearest neighbours of a given state, and obtain:

$$\langle\Psi_{\theta,\phi}| - J\sum_{<i,j>} a_i^\dagger a_j|\Psi_{\theta,\phi}\rangle = -JN_l z\rho_{\mathrm{MF}} = -\frac{N_l}{2}\sin^2\theta\,(3 + 2\sqrt{2})\cos^2\theta\,Jz\ . \tag{86}$$

4.4. Contribution of the on–site interaction energy

The on–site interaction term may be calculated from the following on–site average:

$$\langle\Psi_{\theta,\phi}|n_i(ni-1)|\Psi_{\theta,\phi}\rangle = \langle\chi^{(i)}|n_i(ni-1)|\chi^{(i)}\rangle\ . \tag{87}$$

We first calculate $n_i(n_i-1)\,|\chi^{(i)}\rangle = \sqrt{2}\sin\theta e^{i\phi}\,|2\rangle$, and then $\langle\chi^{(i)}|\,n_i(n_i-1)\,|\chi^{(i)}\rangle = \sin^2\theta$. Each site contributes equally to the total energy, therefore:

$$\langle\Psi_{\theta,\phi}|\frac{U}{2}\sum_{i=1}^{N_l} n_i(n_i-1)|\Psi_{\theta,\phi}\rangle = \frac{N_l}{2}\sin^2\theta\,U\ . \tag{88}$$

4.5. Total energy and second–order phase transition

Combining Eqs. 86 and 88, we finally obtain:

$$\epsilon(\theta) = \frac{2}{N_l z J} \langle \Psi_{\theta,\phi} | H | \Psi_{\theta,\phi} \rangle = \sin^2\theta \left(\frac{U}{zJ} - (3+2\sqrt{2})\cos^2\theta \right) . \tag{89}$$

Equation 89 shows that the phase of the system depends on whether $U/(zJ)$ is greater or smaller than the critical value $3+2\sqrt{2}$.

If $U/(zJ) > 3+2\sqrt{2}$, the term in the parentheses in Eq. 89 is always positive, and $\epsilon(\theta)$ reaches its minimum value 0 for $\theta = 0$. Hence, the system is in the Mott–Insulator phase, with $\psi = 0$.

On the other hand, if $U/(zJ) < 3+2\sqrt{2}$, we introduce the angle θ_0 such that $\cos(2\theta_0) = U/[zJ(3+2\sqrt{2})]$. Then, $\epsilon(\theta)$ is minimal for $\theta = \theta_0$. The order parameter $\psi = (1/\sqrt{2}+1)\sin(2\theta_0)e^{i\phi}/2$ is nonzero, meaning that the system is in the superfluid phase. The energy $\epsilon(\theta_0) = -(3+2\sqrt{2})\sin^4(\theta_0) < 0$ being negative confirms that the superfluid phase is energetically favoured compared to the Mott–Insulator phase (whose energy is 0).

The energy is continuous at the critical point $U/(zJ) = 3+2\sqrt{2}$ (where $\epsilon = 0$), which indicates that we are dealing with a second–order phase transition.

Furthermore, this energetical analysis confirms that there is no constraint on the phase ϕ. The choice of the value of ϕ when entering the superfluid phase is an example of a broken symmetry. Buckling and the para–to–ferromagnetic transition, which are both second–order transitions as well, are also associated with broken symmetries.

5. Question 14: Time–of–flight expansion and Bragg diffraction

In the experiments by Greiner and coworkers [4, 5] analysed in this problem, the coherence between the lattice sites was probed using a frequently used technique known as "time–of–flight" (ToF). At the time t_M at which the measurement should be performed, the optical lattice is suddenly switched off. Then, the matter waves associated with each lattice site are no longer confined, so that they freely expand and interfere. After an expansion time T_{ToF} which is chosen sufficiently long for the waves from all sites in the sample to overlap, the spatial density of the gas is imaged, leading to the experimental interferograms of Figs. 2 and 4 in the problem set.

This time–of–flight protocol affords a straightforward analysis if two conditions are met: *(i)* The expansion is sufficiently long for the initial size of the cloud (before its expansion) to be negligible; *(ii)* The interactions between the particles are sufficiently weak for their role to be negligible at all times during the expansion phase (though interactions are not negligible in the presence of the lattice for $t < t_M$). We shall assume both of these conditions to be satisfied in the following.

5.1. Time–of-flight expansion starting from a lattice potential

Under these two conditions, turning off the lattice causes the atoms to expand from their initial position $\boldsymbol{r} \approx 0$ with a momentum $\hbar\boldsymbol{k}$, i.e. a velocity $\hbar\boldsymbol{k}/m$, which remains unchanged in the course of the expansion. Hence, at atom which is at the final position $\boldsymbol{r}_f$ at the end of the expansion had a momentum $\hbar\boldsymbol{k}$ just before the lattice was turned off which satisfies the relation:

$$\boldsymbol{r}_f = \frac{\hbar\boldsymbol{k}}{m} T_{\mathrm{ToF}} . \tag{90}$$

Equation (90) shows that probing the final density distribution $n_f(\boldsymbol{r})$ at the end of the expansion amounts to probing the momentum distribution $n(\boldsymbol{k})$ just before the expansion, in direct analogy with optical diffraction experiments. Therefore, we now focus on the momentum distribution $n(\boldsymbol{k}) = a^\dagger_{\boldsymbol{k}} a_{\boldsymbol{k}}$, and more precisely on its average $\langle n(\boldsymbol{k}) \rangle$.

In order to characterise this momentum distribution, we must relate the creation operator $a^\dagger_{\boldsymbol{k}}$ for a particle with the momentum $\hbar\boldsymbol{k}$ to the creation operators $a^\dagger_{\boldsymbol{j}}$ for a particle in the lattice site

$\boldsymbol{j}$. Thus, we must relate the wavefunction for the single–particle momentum state $|\boldsymbol{k}\rangle$ to that of a single particle in the lattice site $|\boldsymbol{j}\rangle$:

$$|\boldsymbol{k}\rangle = \sum_{\boldsymbol{j}} \langle \boldsymbol{j}|\boldsymbol{k}\rangle \ . \tag{91}$$

The state $|\boldsymbol{k}\rangle$ is related to the continuum position state $|\boldsymbol{r}\rangle$ through the plane–wave matrix element $\langle \boldsymbol{r}|\boldsymbol{k}\rangle = \exp(i\boldsymbol{k}\cdot\boldsymbol{r})/\sqrt{V}$, so that it is enough to relate $|\boldsymbol{r}\rangle$ to the lattice site wavefunction $|\boldsymbol{j}\rangle$:

$$|\boldsymbol{k}\rangle = \sum_{\boldsymbol{j}} \int d^3r \, \langle \boldsymbol{j}|\boldsymbol{r}\rangle \, \langle \boldsymbol{r}|\boldsymbol{k}\rangle \quad = \sum_{\boldsymbol{j}} \int d^3r \, \langle \boldsymbol{j}|\boldsymbol{r}\rangle \, \frac{\exp(i\boldsymbol{k}\cdot\boldsymbol{r})}{\sqrt{V}} \ . \tag{92}$$

The wavefunction $\langle \boldsymbol{j}|\boldsymbol{r}\rangle$ is localised on the site $\boldsymbol{j}$:

$$\langle \boldsymbol{r}|\boldsymbol{j}\rangle = w_{0\boldsymbol{j}}(\boldsymbol{r}) \quad = w_0(\boldsymbol{r}-\boldsymbol{r}_{\boldsymbol{j}}) \ , \tag{93}$$

where the second step follows from the discrete translational invariance of the lattice, and $\boldsymbol{r}_{\boldsymbol{j}}$ is the spatial position of the lattice site $\boldsymbol{j}$. The function $w_{0\boldsymbol{j}}(\boldsymbol{r}) = w_0(\boldsymbol{r}-\boldsymbol{r}_{\boldsymbol{j}})$ is the Wannier function corresponding to the lowest–energy band and the site $\boldsymbol{j}$, and it may be chosen real (see Sec. 1.2). Combining Eqs. (92) and (93), we obtain:

$$|\boldsymbol{k}\rangle = \sum_{\boldsymbol{j}} \, |j\rangle \int d^3r \, w_0^*(\boldsymbol{r}-\boldsymbol{r}_{\boldsymbol{j}}) \frac{e^{i\boldsymbol{k}\cdot\boldsymbol{r}}}{\sqrt{V}} \quad = \sum_{\boldsymbol{j}} \, |j\rangle \exp(i\boldsymbol{k}\cdot\boldsymbol{r}_j) \int d^3r \, w_0^*(\boldsymbol{r}-\boldsymbol{r}_{\boldsymbol{j}}) \frac{e^{i\boldsymbol{k}\cdot(\boldsymbol{r}-\boldsymbol{r}_{\boldsymbol{j}})}}{\sqrt{V}} \ . \tag{94}$$

Finally, a change of variables in the integral on the right–hand side of Eq. (94) yields:

$$|\boldsymbol{k}\rangle = \left(\sum_{\boldsymbol{j}} \, |j\rangle \, e^{i\boldsymbol{k}\cdot\boldsymbol{r}_{\boldsymbol{j}}} \right) \, w_0^*(\boldsymbol{k}) \ , \qquad \text{with} \quad w_0^*(\boldsymbol{k}) = \langle \boldsymbol{j}=\boldsymbol{0}|\boldsymbol{k}\rangle \ . \tag{95}$$

The form of Eq. (95) is familiar from the theory of the optical diffraction by a periodic grating. It is the product of two terms: the first one describes the interference of plane waves originating from all lattice sites, whereas the second one is the Fourier transform $w_0(\boldsymbol{k})$ of the Wannier function $w_0(\boldsymbol{r})$ associated with the single site at $\boldsymbol{r}=\boldsymbol{0}$.

Recalling that creation operators transform like kets, Eq. (95) directly translates into a relation between the creation operators $a_{\boldsymbol{k}}^\dagger$ and $a_{\boldsymbol{j}}^\dagger$:

$$a_{\boldsymbol{k}}^\dagger = \left(\sum_{\boldsymbol{j}} \, a_{\boldsymbol{j}}^\dagger \, e^{i\boldsymbol{k}\cdot\boldsymbol{r}_{\boldsymbol{j}}} \right) \, w_0^*(\boldsymbol{k}) \ . \tag{96}$$

This yields the following expression for the number operator $n_{\boldsymbol{k}}$:

$$n_{\boldsymbol{k}} = |w_0(\boldsymbol{k})|^2 \sum_{\boldsymbol{j},\boldsymbol{j}'} e^{i\boldsymbol{k}\cdot(\boldsymbol{r}_{\boldsymbol{j}}-\boldsymbol{r}_{\boldsymbol{j}'})} \ a_{\boldsymbol{j}}^\dagger a_{\boldsymbol{j}'} \ . \tag{97}$$

Finally, we average Eq. (97) over multiple realisations of the experiment to obtain:

$$\langle n_{\boldsymbol{k}} \rangle = |w_0(\boldsymbol{k})|^2 \sum_{\boldsymbol{j},\boldsymbol{j}'} e^{i\boldsymbol{k}\cdot(\boldsymbol{r}_{\boldsymbol{j}}-\boldsymbol{r}_{\boldsymbol{j}'})} \ \rho_{\boldsymbol{j}\boldsymbol{j}'} \ , \quad \text{with} \quad \rho_{\boldsymbol{j}\boldsymbol{j}'} = \langle a_{\boldsymbol{j}}^\dagger a_{\boldsymbol{j}'} \rangle \ . \tag{98}$$

5.2. Application to the superfluid–to–Mott insulator transition

5.2.1. Expansion from the Mott insulator phase

We first consider a time–of–flight expansion starting from a trapped gas in the Mott insulator phase. Then, the order parameter $\psi = 0$, meaning that the one–body density matrix $\rho_{\boldsymbol{j}\boldsymbol{j}'} = 0$ for

all $\boldsymbol{j} \neq \boldsymbol{j'}$. Therefore, the only surviving terms in the sum of Eq. (98) are those for which $\boldsymbol{j} = \boldsymbol{j'}$. Then, $\rho_{\boldsymbol{jj}} = \langle n_{\boldsymbol{j}} \rangle = 1$ for all sites $\boldsymbol{j}$. Thus, the momentum–space density distribution satisfies:

$$\langle n_{\boldsymbol{k}} \rangle = |w_0(\boldsymbol{k})|^2 \, N_l \ . \tag{99}$$

It is proportional to the total number N_l of lattice sites, reflecting the incoherent sum of the plane waves in Eq. (98). It gives rise to the incoherent background visible on Figs. (2g,f) of the problem set, whose spatial structure is dictated by the Fourier transform $w_0(\boldsymbol{k})$ of the Wannier function $w_{0\boldsymbol{j}}$ related to the lowest band and any given lattice site $\boldsymbol{j}$.

5.2.2. Expansion from the superfluid phase

In the superfluid phase, the system exhibits long–range order. The ansatz of Eq. (81) leads to:

$$\text{Diagonal elements: } \rho_{\boldsymbol{jj}} = 1 \ , \qquad \text{off–diagonal elements: } \rho_{\boldsymbol{jj'}} = |\psi|^2 > 0 \ . \tag{100}$$

Hence, Eq. (98) reduces to:

$$\langle n_{\boldsymbol{k}} \rangle = |w_0(\boldsymbol{k})|^2 \left(N_l(1 - |\psi|^2) \quad + \quad |\psi|^2 \sum_{\boldsymbol{j},\boldsymbol{j'}} e^{i\boldsymbol{k}\cdot(\boldsymbol{r_j} - \boldsymbol{r_{j'}})} \right) \ . \tag{101}$$

In Eq. (101), the first term inside the parentheses, which is proportional to N_l, reflects the difference $1 - |\psi|^2 > 0$ between the diagonal and off–diagonal values of the one–body density matrix (see Eq. (100)). The double sum over $\boldsymbol{j}, \boldsymbol{j'}$ is the squared modulus of $\sum_{\boldsymbol{j}} e^{i\boldsymbol{k}\cdot\boldsymbol{r_j}}$, which is the multidimensional analog of Eq. (38) (in the experiment of Ref. [5], the optical lattice is 3D). Accordingly, the value of $\langle n_{\boldsymbol{k}} \rangle$ depends on whether or not $\boldsymbol{k}$ is a reciprocal lattice vector:

- *If* $\boldsymbol{k}$ *is* not *a reciprocal lattice vector*, then the phases of the plane waves in the sum over $\boldsymbol{j}, \boldsymbol{j'}$ vary very quickly from one site to the next, so that the sum averages to 0. Hence, the density distribution reduces to the incoherent signal $\langle n_{\boldsymbol{k}} \rangle = |w_0(\boldsymbol{k})|^2 N_l(1 - |\psi|^2)$. It has a structure similar to (99), except that it is weighted by $(1 - |\psi|^2)$, so that the background is less important for systems that were prepared deep in the superfluid phase and becomes more prominent for systems initially closer to the Mott–insulator phase, a dependence which is visible on Figs. (2a–f) of the problem sheet.

- *If* $\boldsymbol{k}$ is *a reciprocal lattice vector*, then all plane waves in the sum over $\boldsymbol{j}, \boldsymbol{j'}$ are equal to 1:

  $$\langle n_{\boldsymbol{k}} \rangle = |w_0(\boldsymbol{k})|^2 \left(N_l(1 - |\psi|^2) \quad + \quad N_l^2 |\psi|^2 \right) \approx |w_0(\boldsymbol{k})|^2 |\psi|^2 N_l^2 \ . \tag{102}$$

  A strongly constructive interference effect occurs, and the signal is now proportional to N_l^2 (rather than to N_l in all other cases). Considering that $N_l \sim 10^5$, this is a strong enhancement and leads to very well–defined peaks, in the momentum distribution, which are clearly visible on Figs. (2a–f) of the problem sheet.

The phenomenon whereby reciprocal lattice vectors lead to strong constructive interference and, hence, to well–defined peaks in the momentum distribution, is fully analogous to the Bragg diffraction of e.g. light through periodic gratings [6, §10.2] or X–rays by crystals [7, chap. 6]. The strong–intensity diffraction peaks relate to the reciprocal lattice vectors and, hence, may be analysed to reconstruct the crystal structure. For example, Figs. 2 and 5 of the problem sheet show that, in the experiments of Refs. [4] and [5], the reciprocal lattice of the optical lattice is a square lattice. The lattice whose reciprocal lattice is square is also a square lattice, hence, the optical lattice used in the experiments by Greiner and coworkers was a square lattice.

6. Questions 15–16: coherent state & its sitewise factorisation

The collapse–and–revival experiment of Ref. [4] was performed using a fixed number of atoms $N_a \sim 10^5$ forming a very pure Bose–Einstein condensate inside the lattice. For $t < 0$, the lattice is shallow and the system is deep in the superfluid regime: $U \ll J$, meaning that interactions are negligible, so that all atoms occupy the single–particle ground state of the lattice. This corresponds to the exact many–particle state $|\mathrm{SF}_{N_a}\rangle = a_{\boldsymbol{k}=\boldsymbol{0}}^{\dagger N_a} |\mathrm{vac}\rangle / \sqrt{N_a!}$. This exact many–particle state is difficult to manipulate because it spans all lattice sites.

As anticipated in Sec. 3.2.3 above, we replace the exact many–particle state $|\mathrm{SF}_{N_a}\rangle$ with the approximate state $|\Psi_{\mathrm{coh}}\rangle$ defined by Eq. (72). In contrast to the derivation provided in Sec. 3.2.3, Questions 15 and 16 of the problem set actually suggest starting from Eq. (76) and deriving Eq. (72). This is readily done by replacing $a_{\boldsymbol{k}=\boldsymbol{0}}^{\dagger}$ in Eq. (76) by its expression in terms of the creation operators $a_j^{\dagger}$ on the site j, given by Eq. (54). The single–particle states $|j\rangle$ representing different lattice sites are orthogonal, hence, the corresponding creation operators $a_j^{\dagger}$ commute and one can replace the exponential of the sum in Eq. (76) by a product of exponentials:

$$|\Psi_{\mathrm{coh}}\rangle \quad = e^{-N_l \nu/2} \exp\left(\sqrt{\nu} \sum_{n=0}^{N_l} a_n^{\dagger}\right) |\mathrm{vac}\rangle \quad = \prod_{j=1}^{N_l} \left[e^{-\nu/2} \exp\left(\sqrt{\nu}\, a_j^{\dagger}\right)\right] |\mathrm{vac}\rangle \quad = \prod_{j=1}^{N_l} |\sqrt{\nu}^{(j)}\rangle \ , \tag{103}$$

where $|\sqrt{\nu}^{(j)}\rangle$ is a coherent state on the site j with the average atom number ν.

Replacing the state $|\mathrm{SF}_{N_a}\rangle$ by $|\Psi_{\mathrm{coh}}\rangle$ entails that the atom number is no longer rigorously fixed, but its mean value is N_a and its standard deviation is $\Delta N_a = \sqrt{N_a}$. For $N_a \sim 10^5$, the ratio $\Delta N_A / N_a \approx 5 \times 10^{-3}$, so that the atom number fluctuations are negligible and, to a very good approximation, $|\Psi_{\mathrm{coh}}\rangle$ reproduces the physics of the exact many–body state.

Note that the single–site coherent states $|\sqrt{\nu}^{(j)}\rangle$ do not have a fixed atom number. The average atom number in each site is ν and the fluctuations are $\Delta\nu = \sqrt{\nu}$. The filling factor $\nu = N_a/N_l \approx 3$ in the experiment of Ref. [4]. Hence, $\Delta\nu/\nu = 1/\sqrt{\nu} \approx 0.58$, so that these atom number fluctuations are not negligible. However, this does not invalidate the use of the multiple–site coherent state $|\Psi_{\mathrm{coh}}\rangle$, whose atom number fluctations are indeed small compared to the total atom number N_a.

To sum up, replacing the exact many–particle state, which has a fixed atom number, with the coherent state $|\Psi_{\mathrm{coh}}\rangle$, whose particle number fluctuations are nonzero but very small, allows us to factorise the many–particle state into the product of Eq. (103), where *each term in the product relates to a single lattice site.*

7. Questions 17 & 18: quantum dynamics in a deep lattice

At the time $t = 0$, we abruptly increase the lattice height to such a large value that the tunnelling between lattice sites is completely negligible. Thus, for $t \geq 0$, the coefficient $J = 0$, and the lattice sites evolve independently from each other. The product form for the many–particle wavefunction of Eq. (103) shows that all sites play the same role. Therefore, we focus on a given site j and call its quantum state $|\psi^{(j)}(t)\rangle$.

The many–particle wavefunction is continuous at $t = 0$, hence, just after the abrupt change in the lattice height, $|\psi^{(j)}(t=0)\rangle = |\sqrt{\nu}\rangle$ is the coherent state with the mean atom number ν introduced in Eq. (103). Using the series representation for a coherent state given by Eq. (126), we may rewrite it as a sum over the single–site Fock states n_j:

$$|\psi^{(j)}(t=0)\rangle = e^{-\nu/2} \sum_{n=0}^{\infty} \sqrt{\frac{\nu^n}{n!}}\ |n^{(j)}\rangle \ . \tag{104}$$

The quantum dynamics of $|\psi(t)\rangle$ for $t > 0$ is dictated by the *single–site Hamiltonian* $H^{(j)} = U\hat{n}_j(\hat{n}_j - 1)/2$. Each Fock state $|n^{(j)}\rangle$ in Eq. (104) is an eigenstate of $H^{(j)}$ with the energy

$Un^{(j)}(n^{(j)}-1)/2$, hence, its time evolution reduces to the phase $e^{-iUn^{(j)}(n^{(j)}-1)t/(2\hbar)}$. This leads to the following expression for $|\psi(t)\rangle$:

$$|\psi(t)\rangle = e^{-\nu/2}\sum_{n=0}^{\infty}\sqrt{\frac{\nu^n}{n!}}\exp\left(-i\frac{U}{\hbar}\frac{n(n-1)}{2}t\right)|n\rangle \ . \tag{105}$$

8. Question 19: coherent matter–wave field on each site

The order parameter $\phi(t)$ is a complex number which is defined just like in Question 12: $\phi(t) = \langle\psi(t)|a|\psi(t)\rangle$. We first calculate $a\,|\psi(t)\rangle$:

$$a\,|\psi(t)\rangle = \sqrt{\nu}e^{-\nu/2}\sum_{n=1}^{\infty}\sqrt{\frac{\nu^{n-1}}{(n-1)!}}\exp\left(-i\frac{U}{\hbar}\frac{n(n-1)}{2}t\right)|n-1\rangle \tag{106}$$

$$= \sqrt{\nu}e^{-\nu/2}\sum_{n=0}^{\infty}\sqrt{\frac{\nu^n}{n!}}\exp\left(-i\frac{U}{\hbar}\frac{(n+1)n}{2}t\right)|n\rangle \ . \tag{107}$$

Then, we take the scalar product with $\langle\psi(t)|$:

$$\phi(t) = \sqrt{\nu}e^{-\nu}\sum_{n=0}^{\infty}\frac{\nu^n}{n!}\exp\left[i\frac{U}{\hbar}t\left(\frac{n(n-1)}{2}-\frac{n(n+1)}{2}\right)\right] \tag{108}$$

$$= \sqrt{\nu}e^{-\nu}\sum_{n=0}^{\infty}\frac{\nu^n}{n!}\exp\left(i\frac{U}{\hbar}t\,n\right) \tag{109}$$

$$= \sqrt{\nu}\exp\left[\nu\left(e^{-iUt/\hbar}-1\right)\right] \ . \tag{110}$$

The order parameter $\phi(t)$ exhibits revivals for all integer multiples of the time $t_{\rm rev} = h/U = 2\pi\hbar/U$, in agreement with the revival times for the full quantum state $|\psi(t)\rangle$.

9. Question 23: Schrödinger cat state at $t = t_R/2$

We first rewrite Eq. 105 in terms of t/t_R:

$$|\psi(t)\rangle = e^{-\nu/2}\sum_{n=0}^{\infty}\frac{\nu^{n/2}}{\sqrt{n!}}\exp\left(-i\,2\pi\frac{t}{t_R}\frac{n(n-1)}{2}\right)|n\rangle \ . \tag{111}$$

We consider the time $t = t_R/2$, so that:

$$|\psi(t_R/2)\rangle = e^{-\nu/2}\sum_{n=0}^{\infty}\frac{\nu^{n/2}}{\sqrt{n!}}\exp\left(-i\pi\frac{n(n-1)}{2}\right)|n\rangle \ . \tag{112}$$

Now, we use the relation $e^{-i\pi n(n-1)/2} = [e^{-i\pi/4}e^{in\pi/2} + e^{i\pi/4}e^{-in\pi/2}]/\sqrt{2}$, which is simply a statement on the parity of n. This leads to:

$$|\psi(t_R/2)\rangle = e^{-\nu/2}\sum_{n=0}^{\infty}\frac{\nu^{n/2}}{\sqrt{n!}}\frac{1}{\sqrt{2}}\left[e^{-i\pi/4}e^{in\pi/2} + e^{i\pi/4}e^{-in\pi/2}\right]|n\rangle \tag{113}$$

$$= e^{-\nu/2}\sum_{n=0}^{\infty}\frac{1}{\sqrt{2}}\left[e^{-i\pi/4}\frac{(\sqrt{\nu}e^{i\pi/2})^n}{\sqrt{n!}} + e^{i\pi/4}\frac{(\sqrt{\nu}e^{-i\pi/2})^n}{\sqrt{n!}}\right]|n\rangle \tag{114}$$

$$= \frac{1}{\sqrt{2}}\left[e^{-i\pi/4}\,|\sqrt{\nu}e^{i\pi/2}\rangle + e^{i\pi/4}\,|\sqrt{\nu}e^{-i\pi/2}\rangle\right] \ . \tag{115}$$

Equation 115 shows that $|\psi(t_R/2)\rangle$ is a superposition of two coherent states, both of which contain the same mean number of atoms ν, but with different phases $\pi/2$ and $-\pi/2$. This macroscopic superposition is a Schrödinger–cat state. It is clearly visible on the numerical Fig. 4d.

However, the interference experiment performed by Greiner et al was not sensitive to the full quantum state $|\psi(t)\rangle$ but only to the coherent matter wave field $\phi(t)$. This latter quantity does not show any signature of the superposition state. Instead, Eq. 110 shows that $\phi(t_R/2) = \sqrt{\nu}e^{-2\nu}$. At $t = t_R/2$, the order parameter is exponentially suppressed, in accordance with the absence of observed fringes on Fig. 5d.

10. Question 20: collapse at short times

10.1. Collapse of the order parameter $\phi(t)$

We first calculate the modulus $|\phi(t)|$ of the order parameter $\phi(t)$:

$$|\phi(t)| = \sqrt{\nu}\exp\left[\nu\left(\cos\left(\frac{Ut}{\hbar}\right)-1\right)-i\nu\sin\left(\frac{Ut}{\hbar}\right)\right] = \sqrt{\nu}\exp\left[-\nu\left(1-\cos\left(\frac{Ut}{\hbar}\right)\right)\right] \ . \quad (116)$$

The typical decay time t_c is given by:

$$\nu\left(1-\cos\left(\frac{Ut_c}{\hbar}\right)\right) = 1, \quad \text{that is,} \quad 1-\cos\left(\frac{Ut_c}{\hbar}\right) = \frac{1}{\nu} \ . \quad (117)$$

Assuming that the atom number per site ν is sufficiently large, the collapse occurs for a time which is small compared to t_R and we may expand the cosine to leading order in t/t_R. This leads to:

$$t_c = \sqrt{\frac{2}{\nu}}\frac{\hbar}{U} = \frac{1}{2\pi}\sqrt{\frac{2}{\nu}}\,t_{\rm rev} \ . \quad (118)$$

This is the typical collapse time observed in the experiment, which is sensitive to $\phi(t)$.

10.2. Wash–out of the initial coherent state

The dynamics of $|\psi(t)\rangle$ is richer than that of $\phi(t)$, as previously illustrated by the Schrödinger–cat nature of $|\psi(t_R/2)\rangle$ to which $\phi(t_R/2)$ is insensitive. It is worth pointing out that the typical timescale t_C over which the inital coherent state $|\psi(t=0)\rangle$ gets distorted is not proportional to the same power of ν as the timescale over which $\phi(t_R/2)$ collapses[7].

In Eq. 111, the atom number n follows a Poisson distribution centred on the mean value ν, with the standard deviation $\delta\nu = \sqrt{\nu}$. The timescale t_C characterising the wash–out of the phase of the full quantum state may be estimated by expressing that the phase variation of the oscillation over the width $\delta\nu$ of the atom number distribution is of the order of 2π:

$$\delta\left(2\pi\frac{t_C}{t_R}\frac{n(n-1)}{2}\right) = 2\pi \ . \quad (119)$$

The differential appearing in Eq. 119 should be evaluated for $n = \nu$. We thus obtain:

$$\frac{t_C}{t_R}(\nu-1/2)\delta\nu = 1, \quad \text{that is,} \quad \frac{t_C}{t_R} \approx \nu^{-3/2} \ . \quad (120)$$

For the last step of Eq. 120, we have assumed $\nu \gg 1/2$.

Therefore, the phase of the initial coherent state is washed out over a time which scales with $\nu^{-3/2}$, i.e. faster than the collapse time for $\phi(t)$ (which scales with $1/\nu$). However, this does not at all mean that the quantum coherence is fully lost, as shown by the occurrence of the superposition state at $t = t_R/2$ and the full revival at $t = t_R$.

[7] I thank Pierre Pelletier for his useful comment regarding this point (October 2018).

11. Fig. 4: graphical representation (Husimi function, theory)

This section is a brief comment on Fig. 4 of the problem sheet, which graphically illustrates the quantum dynamics of the state $|\psi(t)\rangle$. The experiment was sensitive only to the mean–field parameter $\phi(t)$, which was measured through a time–of–flight expansion (see Sec. 5). Therefore, the experiment provided no signature of the Schrödinger cat state $|\psi(t_R/2)\rangle$ obtained at half the revival time t_R (see Eq. (115)). We now discuss how this quantum superposition state may be represented graphically through an appropriate *theoretical* analysis of the single–site state $|\psi(t)\rangle = |\psi^{(j)}(t)\rangle$.

The idea is to expand the single–site quantum state, defined by the density matrix ρ, onto a suitable set of quantum states. We know that coherent states play a key role in the theory considered here, hence, we consider the *average value of* ρ in all coherent states $|\beta\rangle$:

$$Q_\rho(\beta) = \frac{1}{\pi}\ \langle\beta|\rho|\beta\rangle\ . \tag{121}$$

For a given ρ, the function $Q_{|\rho\rangle}(\beta)$, called *Husimi function* (see e.g. Ref. [§3.1.3][8]), is defined for all coherent states $|\beta\rangle$, i.e. for all complex numbers β. Its values are real and positive, hence, it is readily rendered graphically (see e.g. Fig. 4 of the problem set). For a pure state $\rho = |\psi\rangle\langle\psi|$, it reduces to $Q_{|\psi\rangle}(\beta) = |\langle\beta|\psi\rangle|^2/\pi$, i.e. it specifies the squared overlap of $|\psi\rangle$ with all coherent states $|\beta\rangle$.

The Husimi function involves only diagonal elements of ρ (or squared overlaps $|\langle\beta|\psi\rangle|$). Nevertheless, thanks to the overcompleteness of the set of coherent states (see Sec. A.3), this function fully characterises the quantum state ρ. Indeed, combining the series representation of coherent states given by Eq. (126) with the definition of Eq. (121), one obtains:

$$Q_\rho(\beta) = \frac{1}{\pi}\sum_{m,n=0}^{\infty}\frac{\beta^{*m}\beta^n}{\sqrt{m!\,n!}}\ \langle m|\rho|n\rangle\ . \tag{122}$$

In Eq. (122), β is a complex number, so that β and β^* may be seen as two independent quantities with respect to which one may take derivatives. All (diagonal and non–diagonal) matrix elements of ρ in the Fock–state basis are then obtained through:

$$\langle m|\rho|n\rangle = \frac{\pi}{\sqrt{m!\,n!}}\frac{\partial^{m+n}Q_\rho(\beta)}{(\partial\beta^*)^m(\partial\beta)^n}\ . \tag{123}$$

Let us now focus on Fig. 4 of the problem set, which represents the Husimi function $Q_{|\psi\rangle}(\beta)$ of the single–site state $|\psi(t)\rangle$ at various times t.

- At the initial time $t = 0$, the site is in the coherent state $|\sqrt{\nu}\rangle$, and Eq. (128) immediately provides $Q_{|\psi(0)\rangle}(\beta) = \exp(-|\beta-\sqrt{\nu}|^2)/\pi$: the Husimi function is a Gaussian centred on $\sqrt{\nu}$ (i.e. on the horizontal axis), with a $1/e$ width of 1 (see Fig. 4a).
- At the revival time $t = t_R$, $|\psi(t_R)\rangle = |\psi(0)\rangle = |\sqrt{\nu}\rangle$, so that Fig. 4g is identical to Fig. 4a.
- At the time $t_R/2$, the site is in the Schrödinger–cat state of Eq. (115), which consists in a quantum superposition of two coherent states: $|\sqrt{\nu}e^{i\pi/2}\rangle$ and $|\sqrt{\nu}\rangle\, e^{-i\pi/2}$. For $\nu = 3$, the distance between the two points $i\sqrt{\nu}$ and $-i\sqrt{\nu}$, both on the imaginary axis ($2\sqrt{3} \approx 3.46$), is greater than the sum of the $1/e$ widths of the Gaussian Husimi functions corresponding to the two coherent states ($2 \times 1 = 2$). Hence, these two components in the Husimi function are well separated and show up as two non–overlapping Gaussians in Fig. 4d.
- For other times, the Husimi function exhibits an intricate pattern, reflecting the quantum dynamics driven by the atomic collisions within a given site (Figs. 4b, c, e, f).

A. Brief reminder on bosonic coherent states

We consider a given single–particle state $|\psi\rangle$ for a bosonic system (or a given mode of the electromagnetic field). We call a the annihilation operator relative to this mode. The (normalised) eigenstates of the operator a, which are multiple–particle states, are called *coherent states*.

A.1. Definition and explicit expression

The operator a is not hermitian, nor does it commute with $a^\dagger$. Hence, the usual diagonalisation theorems are inapplicable. However, its eigenvalue spectrum may be derived from general principles. Let us consider an eigenstate $|\alpha\rangle$ of the operator a corresponding to the eigenvalue α:

$$a\,|\alpha\rangle = \alpha\,|\alpha\rangle \ . \tag{124}$$

We expand $|\alpha\rangle$ onto the Fock–state basis:

$$|\alpha\rangle = \sum_{n=0}^{\infty} c_n\,|n\rangle \tag{125}$$

Combining Eqs. (124) and (125) yields $c_{n+1} = \alpha\,c_n/\sqrt{n+1}$, so that $c_n = c_0\,\alpha^n/\sqrt{n!}$. Finally, the normalisation condition imposes $|c_0|^2 = \exp(-|\alpha|^2)$. Hence, for any complex number α, there is a single normalised coherent state $|\alpha\rangle$ (up to an unimportant phase factor), which reads[8]:

$$|\alpha\rangle = e^{-|\alpha|^2/2} \sum_{n=0}^{\infty} \frac{\alpha^n}{\sqrt{n!}}\,|n\rangle \quad = e^{-|\alpha|^2/2}\,\exp(\alpha\,a^\dagger)\,|\mathrm{vac}\rangle \ . \tag{126}$$

In Eq. (126), the last step follows from the series expansion $e^z = \sum_{n\geq 0} z^n/(n!)$ combined with the expression $|n\rangle = a^{\dagger n}\,|\mathrm{vac}\rangle\,/\sqrt{n!}$ for the number state $|n\rangle$.

Note that the eigenvalue spectrum of a consists of all complex numbers, in stark constrast to hermitian operators whose eigenvalues are all real.

A.2. Particle number statistics

The coherent state $|\alpha\rangle$ is *not* an eigenstate of the number operator $\hat{n} = a^\dagger a$, hence, it does not correspond to a fixed number of particles. Starting from the series expression for $|\alpha\rangle$ in Eq. (126), one finds the following probability distribution for the particle number n:

$$p_n = e^{-|\alpha|^2}\,\frac{|\alpha|^{2n}}{n!} \ . \tag{127}$$

Equation (127) is a Poisson distribution with the mean value $\langle n\rangle = |\alpha|^2$. Hence, its standard deviation is $\Delta n = \sqrt{\langle n\rangle} = |\alpha|$, so that $\Delta n/\langle n\rangle = 1/\sqrt{\langle n\rangle}$. Therefore, if the average particle number $\langle n\rangle$ is sufficiently large, then $\Delta n \ll \langle n\rangle$, meaning that the fluctuations on the particle number are negligible compared to its mean value. In this situation, the coherent state $|\alpha\rangle$ with $|\alpha|^2 = n$ provides a very good approximation to the Fock state $|n\rangle$, and it is often much easier to use (in particular, see Secs. 3.2.3 and 6 above).

[8] Alternately, the state $|\alpha\rangle$ of Eq. (126) being an eigenstate of a may also be seen directly by writing $a\,|\alpha\rangle = e^{-|\alpha|^2/2}[a, \exp(\alpha\,a^\dagger)]\,|\mathrm{vac}\rangle$ and using $[a, f(a^\dagger)] = f'(a^\dagger)$, valid for any function $f(z)$ which may be expanded into a power series in z. The normalisation of the explicit expression on the right–hand side of Eq. (126) may be directly checked using Glauber's formula $e^X e^Y = \exp(X+Y+[X,Y]/2)$, which holds for any operators X and Y such that $[X,[X,Y]] = [Y,[X,Y]] = 0$: apply it first to $X = \alpha\,a$ and $Y = \alpha^* a^\dagger$, then to $X = \alpha^* a^\dagger$ and $Y = \alpha\,a$, and compare the results. Finally, Glauber's formula leads to the alternate form $|\alpha\rangle = \exp(\alpha a^\dagger - \alpha^* a)\,|\mathrm{vac}\rangle$, which involves the unitary operator $D(\alpha) = \exp(\alpha a^\dagger - \alpha^* a)$ called 'displacement operator'.

A.3. Over–completeness

The linearly independent eigenvectors of a hermitian operator are orthogonal. This property does not hold for the operator a. Indeed, considering two coherent states $|\alpha\rangle$ and $|\beta\rangle$ corresponding to the eigenvalues α and β, and using the series expansion of Eq. (126), we find:

$$\langle\alpha|\beta\rangle = \exp[-(|\alpha|^2 + |\beta|^2 - 2\alpha^*\beta)/2] \ , \quad \text{so that:} \quad |\langle\alpha|\beta\rangle|^2 = \exp[-|\alpha-\beta|^2] \ . \tag{128}$$

Equation (128) shows that two coherent states are never exactly orthogonal. However, their overlap is negligible if the difference between their amplitudes is sufficiently large.

We now show that any vector $|\psi\rangle$ may be expanded onto the set of coherent states. More specifically, we show the relation:

$$\frac{1}{\pi}\int d^2\alpha \ |\alpha\rangle\langle\alpha| = \mathbb{1} \ , \tag{129}$$

where the integral $\int d^2\alpha$ is taken over the complete complex plane. For that purpose, we consider the matrix element of the left–hand side of Eq. (129) between the two Fock states $\langle m|$ and $|n\rangle$:

$$\langle m|\left[\frac{1}{\pi}\int d^2\alpha \ |\alpha\rangle\langle\alpha|\right]|n\rangle = \frac{1}{\pi}\int d^2\alpha \, \langle m|\alpha\rangle\langle\alpha|n\rangle \quad = \frac{1}{\pi}\int d^2\alpha \, e^{-|\alpha|^2}\frac{\alpha^m\alpha^{*n}}{\sqrt{m!}\sqrt{n!}} \ . \tag{130}$$

In Eq. (130), the last step follows from the expression $\langle n|\alpha\rangle = e^{-|\alpha|^2/2}\,\alpha^n/\sqrt{n!}$ (see Eq. (126)). We express the integral on the right–hand side of Eq. (130) in polar coordinates:

$$\langle m|\left[\frac{1}{\pi}\int d^2\alpha \ |\alpha\rangle\langle\alpha|\right]|n\rangle = \frac{1}{\pi}\int dr\, r d\theta \, e^{-r^2}\,\frac{r^{n+m}}{\sqrt{m!}\sqrt{n!}}\,e^{i(m-n)\theta} \ . \tag{131}$$

The angular part of the integral of Eq. (131) gives $\int_0^{2\pi} d\theta \, e^{i(m-n)\theta} = 2\pi\,\delta_{nm}$. Hence:

$$\langle m|\left[\frac{1}{\pi}\int d^2\alpha \ |\alpha\rangle\langle\alpha|\right]|n\rangle = \delta_{nm}\int dr\ 2r\,\frac{r^{2n}}{n!}\,e^{-r^2} \ . \tag{132}$$

The change of variables $u = r^2$ finally yields:

$$\langle m|\left[\frac{1}{\pi}\int d^2\alpha \ |\alpha\rangle\langle\alpha|\right]|n\rangle \quad = \delta_{nm}\int du\,\frac{u^n}{n!}\,e^{-u} \quad = \delta_{nm}\,\frac{\Gamma(n+1)}{n!} \quad = \delta_{nm} \ , \tag{133}$$

which completes the proof.

Overcompleteness means that the decomposition onto the set of coherent states is not unique. For example, the vacuum state $|\text{vac}\rangle = |0\rangle$ is the coherent state corresponding to the eigenvalue $\alpha = 0$, may also be expanded thanks to Eq. (129) to obtain:

$$|0\rangle = \frac{1}{\pi}\int d^2\alpha \, e^{-|\alpha^2|/2} \ |\alpha\rangle \ . \tag{134}$$

References

[1] I. Bloch, J. Dalibard, W. Zwerger, Rev. Mod. Phys. **80**, 885 (2008).

[2] I. Bloch, M. Greiner, Adv. At. Mol. Opt. Phys. **52**, 1 (2005).

[3] P. G. de Gennes, *Superconductivity of metals and alloys*, Perseus (1966).

[4] M. Greiner, O. Mandel, T. W. Hänsch, I. Bloch, Nature **419**, 51 (2002).

[5] M. Greiner, O. Mandel, T. Esslinger, T. W. Hänsch, I. Bloch, Nature **415**, 39 (2002).

[6] E. Hecht, *Optics*, Pearson, 5th ed. (2017).

[7] N. W. Ashcroft, N. D. Mermin, *Solid State Physics*, Harcourt (1976).

[8] S. Haroche, J. Raimond, *Exploring the quantum*, Oxford University Press (2006).